2016

Far-Field Impacts of Tidal Energy Extraction and Sea Level Rise in the Gulf of Maine

Boma Kresning
University of Rhode Island, boma_kresning@my.uri.edu

FAR-FIELD IMPACTS OF TIDAL ENERGY EXTRACTION AND SEA LEVEL RISE IN THE GULF OF MAINE

BY

BOMA KRESNING

A THESIS SUBMITTED IN PARTIAL FULFILLMENT OF THE

REQUIREMENTS FOR THE DEGREE OF

MASTER OF SCIENCE

IN

OCEAN ENGINEERING

UNIVERSITY OF RHODE ISLAND

2016

MASTER OF SCIENCE THESIS

OF

BOMA KRESNING

APPROVED:

Thesis Committee:

Major Professor M. Reza Hashemi

Jason Dahl

John W. King

Nasser H. Zawia

DEAN OF THE GRADUATE SCHOOL

UNIVERSITY OF RHODE ISLAND

2016

ABSTRACT

The dynamics of tides in the Gulf of Maine are unique due to the tidal resonance, which generates the largest tidal range in the world (about 16 m). Consequently, a large tidal energy resource is available in this area, particularly in the Bay of Fundy, and is expected to be harvested in the future. Currently, more than 6 projects are operational or under development in this region (in both US and Canadian waters). Understanding the far-field impacts of tidal-stream arrays is important for future development of tidal energy extraction. The impacts include possible changes in water elevation, currents, and sediment transport. Accordingly, a number of previous studies have assessed the impacts of the tidal energy development in the Gulf of Maine. Further, due to the sea level rise (SLR), those impacts may also change during the project lifetime, which is usually more than 25 years. The objective of this study is to assess the combined effects of SLR and tidal energy extraction on the dynamics of tides in the Gulf of Maine.

A tidal model of the Gulf of Maine was developed using Regional Ocean Model System (ROMS) at one arcminute scale. The model extends from 71.5W to 63.0W and from 39.5N to 46.0N. After validation of the model at NOAA tidal gauge stations and NERACOOS buoys, several scenarios; including SLR scenario, and tidal extraction scenario, were examined. Recent studies suggest that the global dynamics of tides will change due to SLR; therefore, SLR not only affects the bathymetry of the model inside the domain, it also changes the boundary forcing, which was considered in this effort. The results of the impacts of the tidal energy extraction with and without the SLR were presented, and compared with those from literature. Up to 4% decrease in tidal range and M2 amplitude was estimated in Minas Basin due to the 2.5 GW extraction scenario without SLR. On Massachusetts coastal area, the impacts of the same scenario can be considered

negligible, 0.94%. In summary, the implementation of modified boundary forcing due to SLR, which was ignored in the previous works, can change the results of the impact assessment. Based on the results, the far-field impact is more threatening in coastal regions of US. However, the impact of energy extraction in Minas Passage is relatively small. Compared to the model validation, the impacts were inside the uncertainty level of the model. For example, maximum change in Boston coastal area was calculated up to 1.65 %, which is inside the level of uncertainty in models, about 10 %. Furthermore, the impact of SLR on the dynamics of tides is much more than energy extraction assuming 2.5 GW extraction in Minas Passage.

ACKNOWLEDGMENTS

First, I would like to acknowledge my Major Professor, M. Reza Hashemi for his continuous support, guidance, and help of this thesis. Also, I want to appreciate my other committee members, Jason Dahl, John King, Malcolm Spaulding and Huijie Xue for their input in my thesis. Additionally, a thank you for Matias Green and Sophie B. Williams from Bangor University, Wales for their support in global change in tidal dynamics data for this thesis. Lastly, I would like to acknowledge my colleagues in ocean engineering URI, Michael Shelby and Lauren Schambach for their assistance. Thank you for a great time in Ocean Engineering URI.

TABLE OF CONTENTS

Page

Page

LIST OF TABLES

Table **Page**

LIST OF FIGURES

Figure **Page**

Figure **Page**

CHAPTER 1

Introduction

1.1 Background

Ocean renewable energy resources (e.g, tidal range and tidal-stream) can help reduce carbon emissions, which are produced by fossil fuel based power plants (Pelc and Fujita, 2002). Currently, ocean renewable energy extraction is in the development phase from prototype design into commercial power generation.

Tidal energy generation is highly site-specific and generally is feasible where the tidal range and/or current velocity are large enough due to the ocean environment such as amplification by the sea bottom profile, estuaries profile, reflections by large peninsulas and headlands, and resonance effects (Frau, 1993). The Gulf of Maine, which is located in the north east of America continent, has a vast amount of energy due to the resonance effect. Previous studies in this area have explored the available tidal energy resource and also some researchers have assessed the impacts of energy extraction on the marine environment. Additionally, recent studies (e.g., Nicholls and Cazenave, 2010) shows the importance of the SLR scenario in ocean modeling due to its potential impacts on ocean dynamics. In this research, the impact of tidal energy extraction considering SLR was simulated to predict future change in the dynamics of tides.

1.2 Area of study

The study area extends from 71° W to 63° W and 41° N to 46° North. The domain is selected to simulate the Gulf of Maine system including the continental shelf of North America. Figure 1.1 shows the model domain in this study.

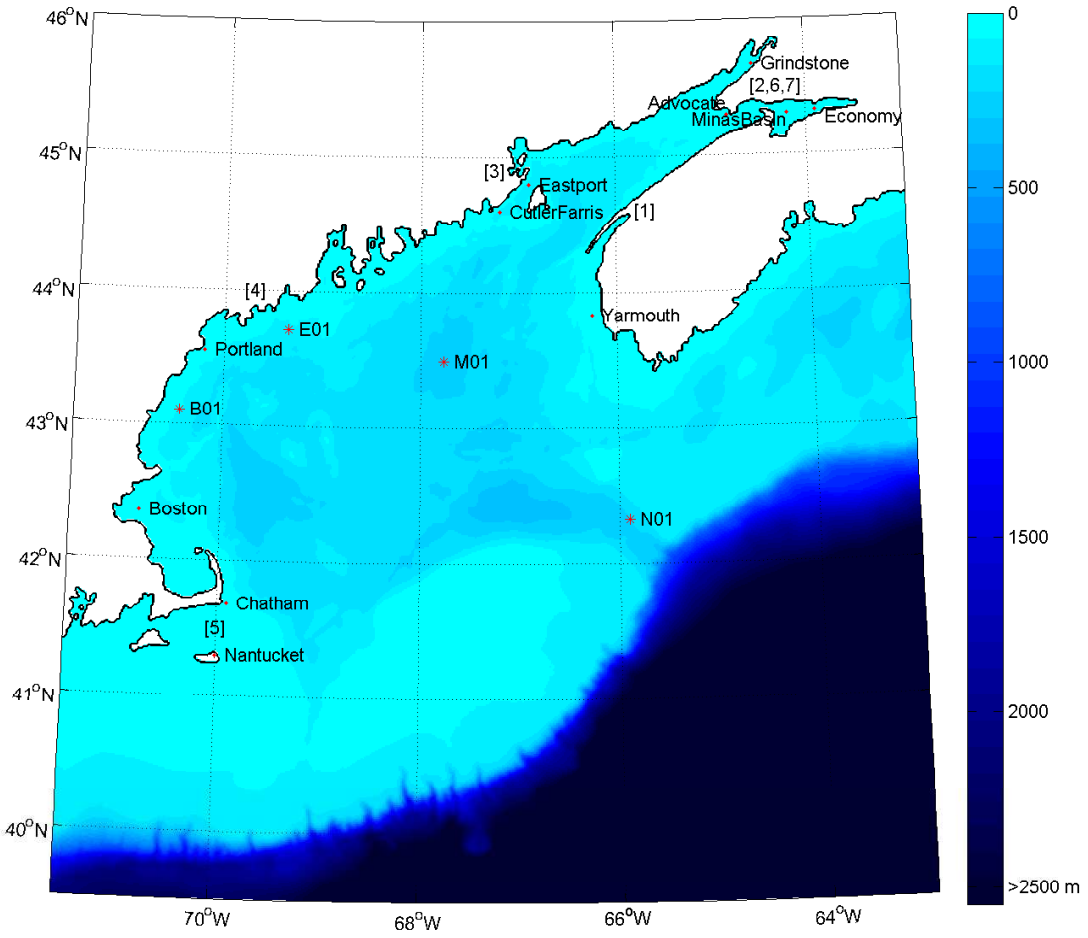

Figure 1.1. Map of the Gulf of Maine including the bathymetry. Red stars show tidal stations for sea level data, red triangles show NERACOOS buoys and numbers show previously studied sites. See Table 1.3 for list of projects.

1.3 Literature review

1.3.1 Tidal energy development

Tides are highly predictable which make them a reliable source for power generation. Tidal energy generation can be categorized into two methods: tidal barrages/lagoons, and tidal energy converters (TEC). Tidal barrages/lagoons benefit from the tidal range, while TEC rely on the tidal current velocity. Further, tidal barrages/lagoons technology is relatively well-developed method for tidal energy generation, while TEC technology is fairly new (Esteban and Leary, 2012; Rourke et al., 2010; Pelc and Fujita, 2002). Table

1.1 displays tidal barrage/lagoon projects worldwide. On the other hand, tidal-stream technology is currently developing from prototype scale into practical use (Rourke et al., 2010). Table 1.2 presents tidal-stream energy development by leading tidal-stream turbine companies: SeaGen (www.seageneration.co.uk), Atlantis (www.atlantisresourcescorporation.com), Marine Current Turbine (www.marineturbines.com), and Open Hydro (www.openhydro.com).

Table 1.1. Some of the tidal barrage/lagoon projects worldwide (Multon, 2013)

Country	Plant	Total output	Annual production	Commissioning year	Reservoir surface area (km^2)	Average tidal range (m)
France	La Rance	240 MW	540 GWh	1966	22	8.5
Canada	Annapolis	20 MW	50 GWh	1984	15	6.4
China	Jiangxia	3.2 MW	11 GWh	1980	1.4	5
Russia	Kislaya Guba	1.9 MW	Unknown	1968	1.1	2.3
South Korea	Sihwa	254 MW	550 GWh (estimated)	2011	43	5.6

Table 1.2. Some important tidal-stream projects in the world (Bahaj, 2011)

Company	Project Location	No. of machines	Status
Marine Current Turbine	SeaGen, UK	1	Operational, 2008
	The Skerries, UK	7	Testing, 2013/14
	Bay of Fundy, Canada	No data	No data
	Kyle Rhea, UK	4	Testing, 2013
	Brough Ness, UK	66	Deployment plan, 2017/2020
	Antrim, UK	100	Deployment plan, 2018
Open Hydro	EMEC, UK	No data	Testing, 2006
	Bay of Fundy, Canada	No data	Damaged, removed 11/6/2010
	Alderney, UK	No data	No data
	Cotes d'Armor, France	4	Testing, 2011/12
	Scotland, UK	No data	Deployment Plan 2020
Atlantis	EMEC, UK	1	Aug 2010. Withdrawn (Nov 2010) due to total parting of the composite material from blade structures.
	Project Blue, UK	30	No data

Tidal stream technology has been inspired largely by the wind turbine technology. TEC is categorized into horizontal and vertical axis turbines (Figure 1.2). The present available TEC in the market are dominated by the horizontal axis turbine (e.g., SeaGen S by Marine Current Turbine). SeaGen S is designed with a 20 m rotor diameter, up to 38 m water depth deployment, and 1.0 o 2.5 m/s tidal current velocity. Figure 1.3 shows the power curve for the SeaGen S. The

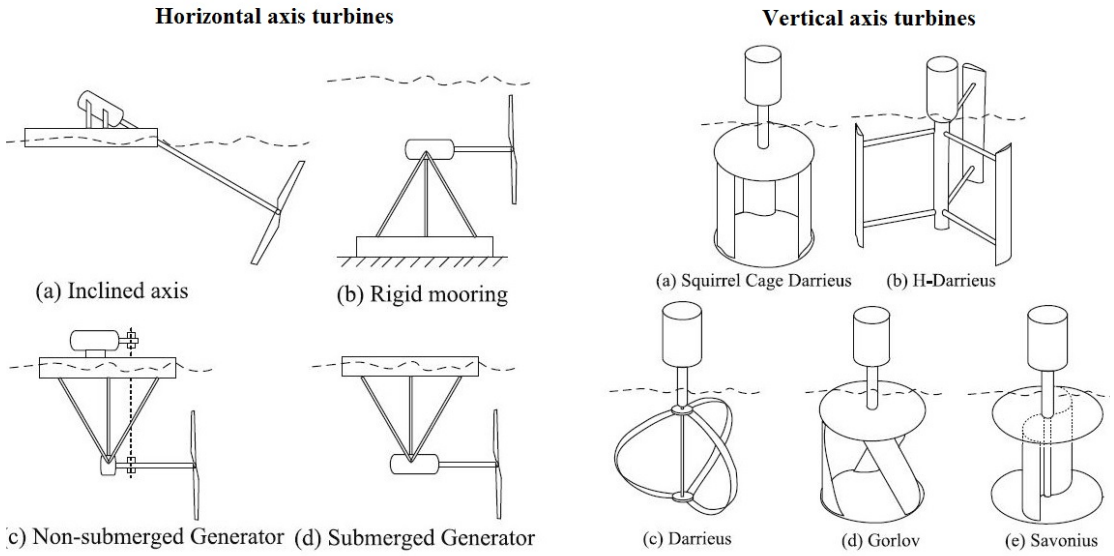

Figure 1.2. Illustration of stream turbine types (Khan et al., 2009).

company reported that the device is capable of generating up to 20 MWh per day with a maximum of 1100 kW energy extraction capacity.

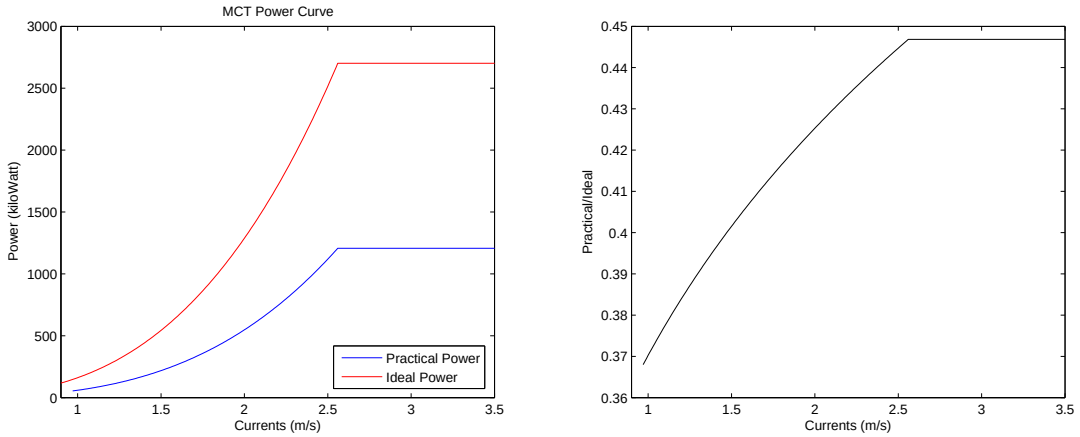

Figure 1.3. Power curve for the SeaGen-S tidal stream turbine by Marine Current Turbine.

Present day turbine technology, which is designed for ∼2.5 m/s maximum tidal current velocity and water depth ranging from 25 and 50 m, are categorized as the first generation of TEC and are expected to lead tidal-stream energy generation within the next 10 years (Iyer et al., 2013). A recent study by Lewis et al. in 2015

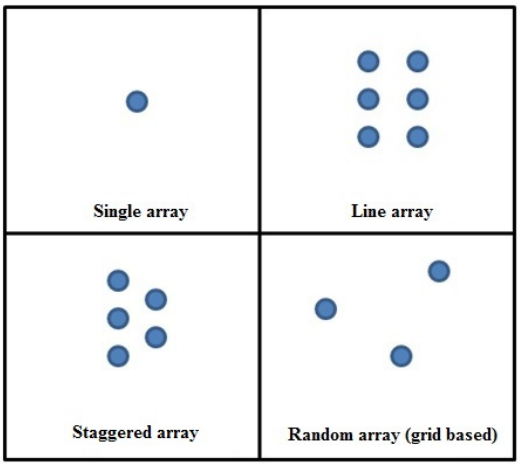

Figure 1.4. Illustration of tidal-stream turbine arrays (Divett et al., 2013; Chowdhury et al., 2013).

considered future TEC generations based on maximum tidal current velocity and water depth in their simulation. In the cited study, second and third generation of TEC are expected to aim towards a lower tidal current velocity limit. In details, limits for those turbines are: first generation (velocity $>$ 2.5 m/s 25 $<$ h $<$ 50); second generation (velocity $>$ 2 m/s & h $>$ 25 m); third generation (velocity $>$ 1.5 m/s & h $>$ 25 m).

TEC must be placed in a specific array configuration in order to optimize energy extraction. Wake effects from the blades disturb water flow in an array. Thus, TEC array optimization must consider the wake effects to maximize energy extraction. Figure 1.4 illustrates possible tidal-stream turbine arrays in the ocean: single turbine, line array, staggered array and random (grid based) array. A recent study by Divett in 2013 suggested the staggered array as the most optimal array configuration, which 54% more efficient compared to other configurations . In the cited study, the distance between turbines was suggested as 7.5 and 10 times TEC blade diameter for the across and along the flow field, respectively. Figure 1.5 shows the suggested array configuration.

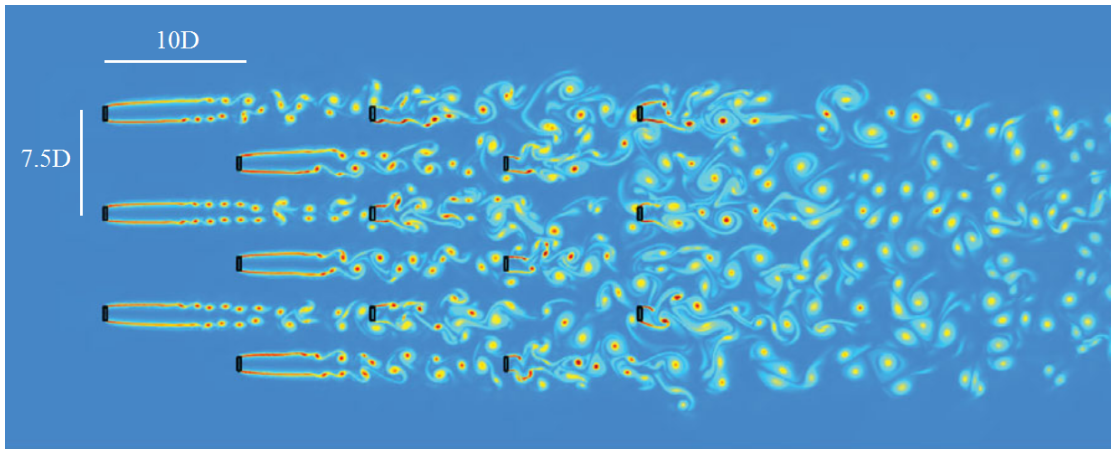

Figure 1.5. Optimum multiple line array configuration with recommended spacing between turbines. Colors represents generated wake from the turbines due to incoming current. Picture redrawn from Divett et. al, 2013.

The environmental impacts of tidal energy generation are important to consider in TEC development. Tidal barrages/lagoons are known to cause problems around their reservoirs, such as sedimentation. The impacts of tidal-stream turbines are mostly unknown. The potential physical impacts of tidal-stream turbine sites may include changes in the dynamics of tides, sedimentation and ecosystem disturbance.

1.3.2 Tidal energy resource in the Gulf of Maine

The Gulf of Maine has one of the highest tidal ranges in the world, 16 m in Minas Basin. Previous studies (Garrett, 1972; Greenberg, 1987; Desplanque and Mossman, 2001) have suggested that the Bay of Fundy and the Gulf of Maine are a unified system that produce resonance due to their geographical configurations. Consequently, the Gulf of Maine has a high potential for ocean renewable energy. A map of Gulf of Maine and previous research results of maximum power generation are shown in Figure 1.6, more details are provided in Table 1.3 for each site.

In terms of tidal energy resource assessment, several locations for both tidal

range and tidal-stream energy generation have been explored by past studies as shown in Figure 1.6. Annapolis Tidal Power Station has been supplying 50 GWh annual electricity productions for Canada since the 1980's (Multon, 2013). Also, there is an upcoming plan of TEC site development by FORCE-Canada with a 4 MW energy extraction project that consists of two 16 m turbine arrays at Cape Sharp, Minas Passage (fundyforce.ca). Other studies have investigated the area for additional sites such as Minas Passage and Gulf of Maine coastal areas. Karsten in 2008 estimated a 6.95 GW potential tidal-stream generation at Minas Passage. A recent study by Cornett in 2013 supported previous research with calculated maximum power generation of 11-24 kW/m^2 at the passage. In the United States coastal areas of the Gulf of Maine, a potential of 0.510 kW/m^2 tidal-stream energy extraction was predicted in several sites. For instance, 2-10 kW/m^2 maximum energy generation was predicted on Passamaquoddy-Cobscook Bay (Brooks, 2006), and 2-6.5 kW/m^2 was simulated on the Kennebec River (Brooks, 2011).

Table 1.3. Tidal energy sites (mostly under study) in the Gulf of Maine.

No	Location/site	Sources	Type	Maximum current speed (m/s)	Maximum theoretical tidal energy (kW/m2)	Average theoretical tidal energy (kW/m2)	Maximum practical tidal energy
1	Annapolis	(Multon, 2013)	Barrage	-	-	-	50 GWh (Annual)
2	Minas Passage	(Bahaj, 2011)	Stream	-	-	-	4 MW
3	Passamaquoddy Cobscook Bay	(Brooks, 2006)	Stream	>4	>10	>5	-
4	Kennebec River	(Brooks, 2011)	Stream	>2	>4	>0.9	-
5	Massachusetts	(Hagerman and Bedard, 2006)	Stream	>2	>4.89	>0.9	-
6	Minas Passage	(Cornett et al., 2010)	Stream	>5	>80	>24	-
7	Minas Basin	(Cornett et al., 2013)	Barrage (single operation, 6 m head)	-	-	265 MW (coastal) 165 MW (offshore)	
	-						

1.3.3 Physical impacts of tidal energy extraction

Extracting energy from the water column will cause changes in the dynamics of the ocean. In the Gulf of Maine, any change that occurs in the dynamics of tides will create effects in the far field (Müller, 2011) due to basin's resonance.

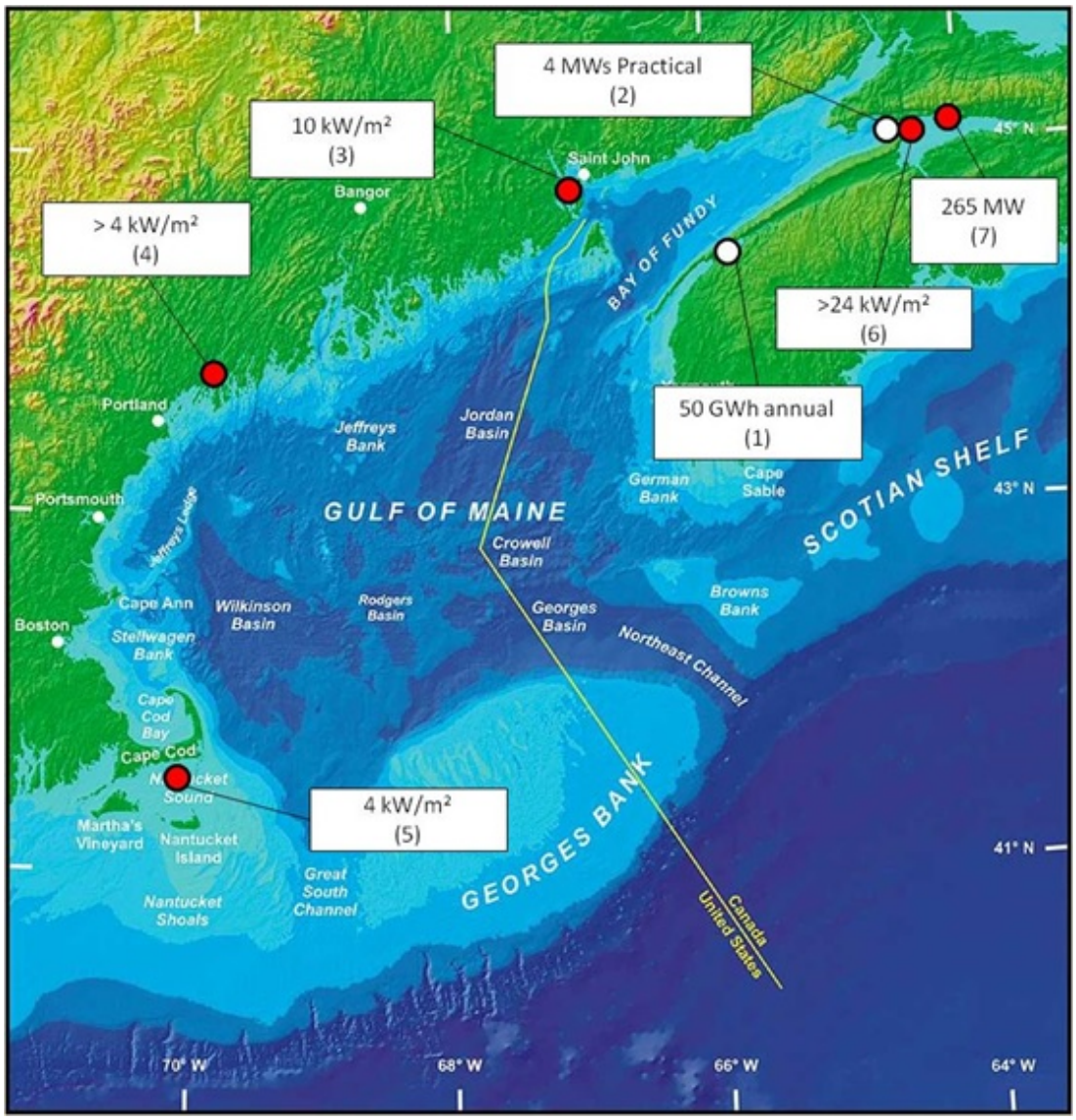

Figure 1.6. Map of Gulf of Maine and previously studied renewable energy sites. The boxes display the maximum resource at location otherwise noted. See Table 1.3 for details. Redrawn from the original images at /www.necwa.org

Several methods have been used in the literature to simulate TEC in ocean models, such as the increasing bottom drag coefficient method and actuator disc theory (Garrett and Cummins, 2005; Roc et al., 2013). Karsten et al., 2008 modeled tidal-stream turbines at $\sim 10 km^2$ area in Minas Passage to set up a 6.95 GW power extraction using the additional bottom friction in Finite-Volume Community

Ocean Model (FVCOM). The cited study predicted a decrease of tidal elevation in Minas Basin by 36%. A recent study by Hasegawa et al., 2011 supported previous research with 7.6 GW tidal-stream extraction scenario using the increasing turbine drag coefficient method in the water column. In the cited study, the maximum tidal current velocity reduction was predicted at 38.8%, the maximum M2 tidal amplitude decrease was simulated up to 2.4 m inside the Bay of Fundy, and 0.2 m M2 amplitude increase is predicted for the Massachusetts coastal area as the results of 7.6 GW tidal-stream extraction scenario.

With regard to tidal-stream energy extraction and SLR, a recent study by Pelling and Mattias Green, 2013 included 2 m SLR to simulate the impact of tidal energy extraction at Minas Passage on the Gulf of Maine. The simulation was performed with a 2-D ocean model with a 1 arc minute grid resolution. The simulated scenario consisted of 7.1 and 5.2 GW tidal-stream energy extraction scenarios, including the consideration of coastal flooding due to SLR. In the cited study, the flood scenario was defined as SLR being allowed to overtake the coastal areas while the no-flood was defined as SLR without coastal flooding. Figure 1.7 displays the results from the cited study. Up to 0.5 m tidal amplitude increase was predicted on Massachusetts coastal area due to the maximum tidal-stream energy extraction scenario (7.1 GW) for both SLR scenarios.

In summary, previous studies (Hasegawa et al., 2011; Karsten et al., 2008; Pelling and Mattias Green, 2013) explored the response of tidal dynamics in the Gulf of Maine to tidal-energy extraction. In general, Tidal stream energy extraction at Minas Passage will decrease the tidal amplitude inside the Bay of Fundy and increase the tidal amplitude in the United States coastal area.

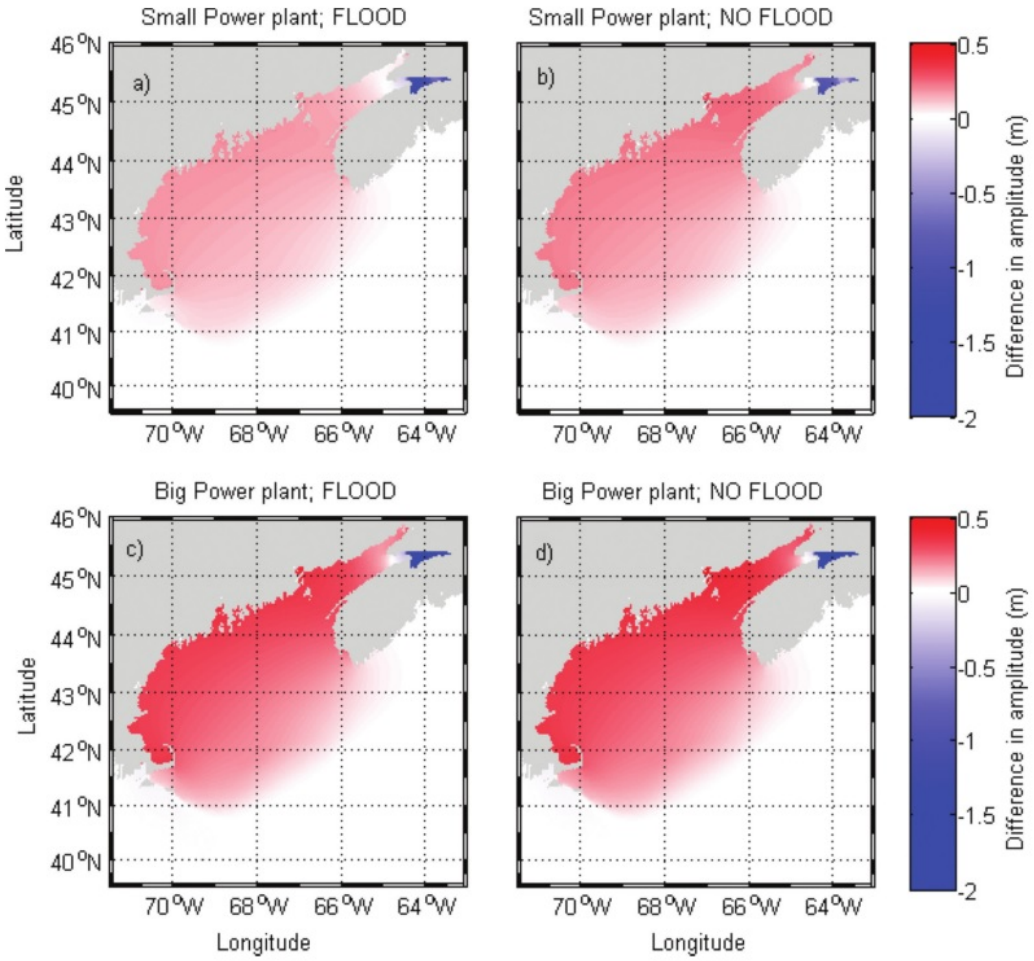

Figure 1.7. Impact of tidal-stream energy extraction and 2 m SLR combined with flood and no flood scenarios (Pelling and Mattias Green, 2013).

1.3.4 Sea level rise

Tides as long waves are easily modified by water depth, bathymetry, and topographic features (Pugh and Woodworth, 2014). Therefore, tidal dynamics is sensitive to SLR, which changes ocean bathymetry and global dynamics of the ocean. NOAA has published a map of global SLR trend which is shown in Figure 1.8. The highest SLR trend, which is up to -10 mm/year rise, is observed in South East Asia while the lowest is measured in the Pacific Ocean at 10 mm/year water elevation decline. For the Gulf of Maine area, SLR trend is reported between 2-6 mm/year. A study by Paris et. al in 2012 predicted SLR projections

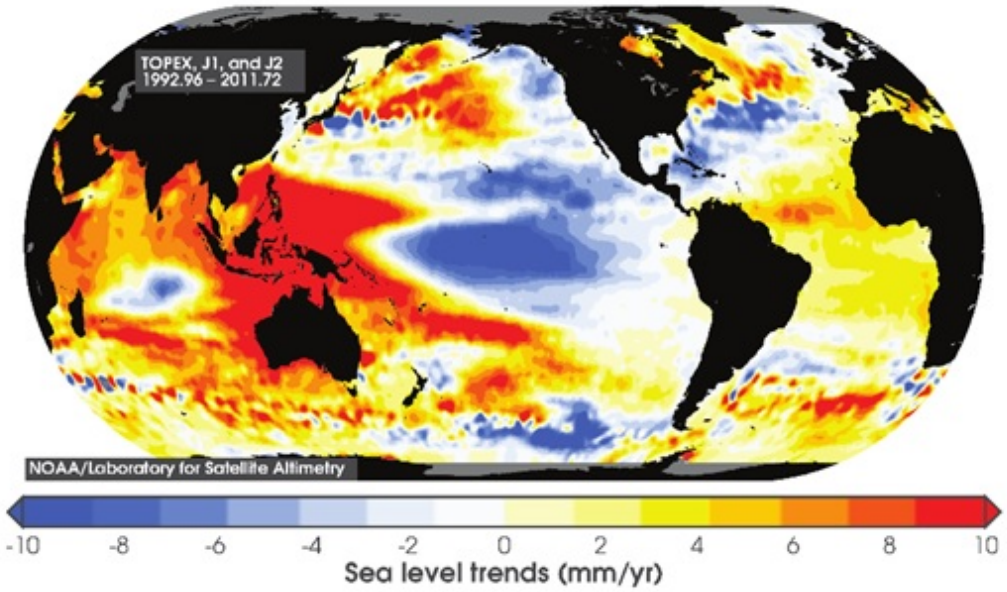

Figure 1.8. Global SLR trend as observed from TOPEX/Poseidon (T/P); Jason-1; and Jason-2 sattelites(NOAA, 2016)

from present day to year 2100 based on the observed global mean sea level trend. Several SLR scenarios were established in the cited study: lowest, intermediate-low, intermediate-high, and highest scenario. Common SLR scenarios for ocean studies are the highest and the intermediate scenarios, which are 2.0 and 1.0 m, respectively. In terms of the impacts of SLR on global tidal dynamics, a recent study using a global ocean model predicted the change on the M2 and K1 components due to SLR (Wilmes, 2016). The cited study presented M2 and K1 amplitude changes due to a globally uniform 1 m SLR, which is shown in Figure 1.10. For the M2 component, the Atlantic Ocean and the North Sea were predicted to experience up to a 10 cm increase while the Pacific and the Indian Oceans were projected to experience a 7.5 cm decrease in amplitude. For K1 components, changes were simulated as between -0.05 to 0.05 cm and likely to occur in coastal areas with a basin configuration. Significant amplitude change for the K1 are in South East China Sea, Sea of Okhotsk, Bering Strait and Arafura Sea. For the Gulf of Maine

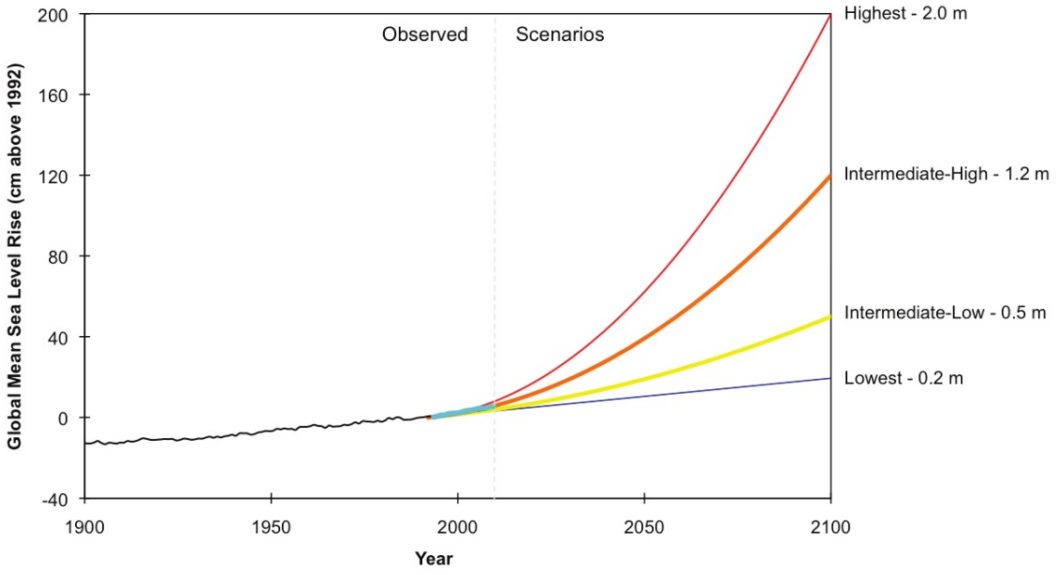

Figure 1.9. SLR predictions and scenarios. (Parris et al., 2012)

continental shelf area, the change in the M2 amplitudes was predicted about 10%. The cited study did not explore the other important tidal components such as the S2 and N2.

1.3.5 Introductory remarks

The Gulf of Maine has very good tidal energy potential due primarily to the extreme tidal range, up to 16 m, in the Bay of Fundy. Therefore, many studies have been conducted to better understand the tidal resource and evaluate the most efficient and effective methods of energy generation, and also to predict the future impacts of energy extraction.

Presently, available TEC devices in industry are mainly horizontal axis turbines designed by several companies such as SeaGen, Marine Current Turbine, and Open Hydro. Further research on TEC also focuses on array optimization. Single turbine, line array, staggered array, and random array designs are possible site optimization method which is based on methods used in offshore wind array.

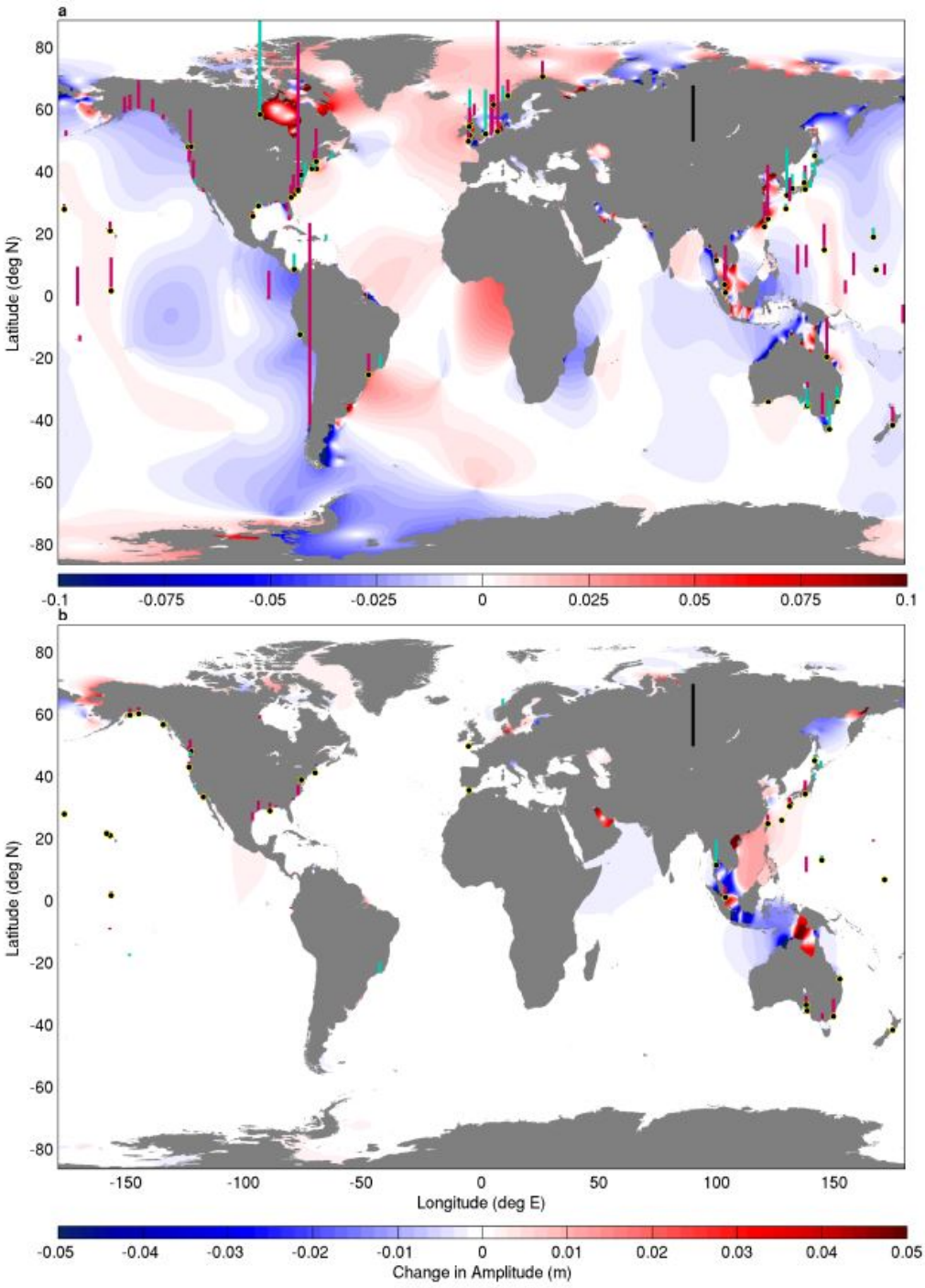

Figure 1.10. Changes in the amplitudes of M2 and K1 components due to 1 m SLR. Picture from Wilmes, 2010.

In terms of tidal energy resources, previous studies have explored several potential areas in the Gulf of Maine for site development. Several narrow channels such as Nantucket Channel, Kennebec River, Passamaquoddy-Cobscook Bay, and Minas Passage are of interest for energy harvesting.

A number of studies have examined the effects of tidal energy extraction in the area. Many of the past studies simulated tidal energy extraction at Minas Passage, which was predicted to have very high tidal-stream velocities (up to 3.5 m/s). In general, previous studies predicted a tidal amplitude decrease inside the Bay of Fundy and a tidal amplitude rise in the US coastal area. Recent research in global ocean dynamics predicted that SLR is not only adding water elevation in the ocean but also changes the boundary forcing. Therefore, SLR may change the impacts of tidal energy extraction.

1.4 Objectives

The objectives in this study can be listed as follows:

1. Assessment of the impacts of the tidal energy extraction on tides in the Gulf of Maine.

2. Investigating the effect of SLR on tidal energy resource, including the changes in global dynamics of tides.

Firstly, this study aims to predict the impacts of tidal power extraction and SLR on the Gulf of Maine. Previous studies have focused on the dynamics of tides, resource assessment, and tidal energy extraction at several sites such as Passamaquoddy-Cobscook Bay, Kennebec River, Minas Passage and Minas Basin. Furthermore, SLR, which is caused by global climate change, has emerged as an important factor that affects the dynamics of tides. Therefore, assessment of the combined effect of tidal energy extraction and SLR on the dynamics of tides pro-

vides a better understanding of the impacts in the future, and will be beneficial to tidal energy development. Furthermore, recent studies in global dynamics of tides suggest that SLR not only affects the bathymetry of the model, it also modifies the boundary forcing. This study will analyze the changes on tidal dynamics due to tidal-stream energy extraction and SLR, including the changes in the dynamics of tide.

CHAPTER 2

Methods

2.1 Data

2.1.1 Bathymetry

The Gulf of Maine bathymetry is provided by United States Geological Survey (USGS) (pubs.usgs.gov) combined with NOAA Coastal Relief Model (maps.ngdc.noaa.gov). A 15 arc second resolution dataset from USGS, which covers 71° West to 63° West and from 39.5° North to 46° North, was used as the core bathymetry data and NOAA Coastal Relief was added to extend the domain.

2.1.2 TPXO7

TPXO is a global solution of ocean tides provided by Oregon State University (OSU) that is modeled numerically based on TOPEX/Poseidon and Jason Satellite observations. The dataset provides eight primary (M2, S2, N2, K2, K1, O1, P1, Q1), two long period (Mf,Mm) and 3 non-linear (M4, MS4, MN4) harmonic constituents. In this study, TPXO7 (volkov.oce.orst.edu), which has 1/4° x 1/4° resolution, was used to generate tidal forcing.

2.1.3 Tidal water elevation and tidal amplitude

Tidal water elevation and tidal components data are commonly used in model validation. In this thesis, 11 stations in the Gulf of Maine was used for validation.

Tidal water elevation was obtained from NOAA website (tidesandcurrents.noaa.gov) that provide historical data, prediction of water elevation for public and amplitude for tidal components. There are 6 NOAA tidal stations in the Gulf of Maine: Portland, Eastport, Nantucket, Boston, Chatham, Cutler Farris which are used in this thesis for model validation. For stations which are located in Canada, tidal amplitude at 5 locations (Yarmouth, Grindstone, Advocate Har-

bour, Minas Basin and Economy) was obtained from previous studies, e.g, Wu, 2011). January-February 2011 period was selected as validation period due to time series data availability at all of the stations.

2.1.4 Tidal current velocity data

Tidal current velocity measurement was retrieved from NERACOOS website (www.neracoos.org). The website provides various measurement from their buoys which are operating in the Gulf of Maine. Due to data availability, we used 4 buoys (M01, N01, B01 and E01) for model validation. Similar to tidal water elevation, historical current measurement data was retrieved for January-February 2011 period.

2.1.5 SLR

Sea level rise data in this thesis were based on the literature study in Section 1.3.4. Model scenarios regarding SLR consider the effect of SLR on bathymetry and boundary effect. Figure 2.1 shows the model domain and the relative changes of the M2 amplitude due to 1 m SLR. The effect of on bathymetry is defined as

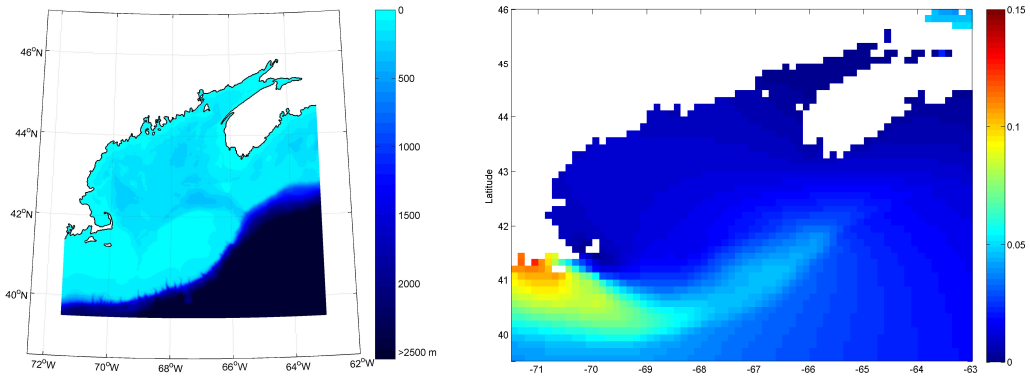

a) b)

Figure 2.1. a) ROMS domain for the Gulf of Maine with color bar shows model bathymetry; b) Relative change in the M2 amplitude due to 1 m SLR (Wilmes, 2016).

uniform +1 m water elevation without coastal flooding and the boundary effect is

defined as 10% increase in M2 amplitude along the open ocean boundary.

2.2 Methodology

The methodology used in this work to examine the impacts of tidal-stream energy extraction and SLR follows these steps:

- Application of a tidal model for the area using Regional Ocean Model System (ROMS).
- Model validation.
- Tidal stream resources assessment assuming present situation.
- Impact of SLR on tidal stream resources.
- Impact of tidal-stream energy extraction and SLR on the dynamics of tides.

2.3 Theoretical background

2.3.1 Tidal constituents

Tidal constituents are key parameters in tidal modeling. 45 astronomical and 101 shallow-water constituents are known and are implemented in t_tide (Pawlowicz et al., 2002). However, many of them have small amplitudes and/or extremely long periods. Therefore, in this thesis, 10 dominant tidal constituents are used for tidal simulation, as shown in Table 2.1.

2.3.2 Resonance in a basin

Tides can be regarded as long waves. Further, waves in the ocean are modified by water depth and coastal boundaries. Wave transformations, such as shoaling, refraction, and diffraction, apply to propagating waves in the ocean. Aside from that, coastal boundaries reflect incoming waves, causing interaction between the incident and reflected waves. This phenomenon may lead to standing waves, an

Table 2.1. 10 Significant Tidal Constituents

Tidal Constituent		Period (hr)	Speed (°/hr)
M2	Principal lunar semidiurnal	12.42	28.984
S2	Principal solar semidiurnal	12.00	30.000
N2	Larger lunar elliptic semidiurnal	12.65	12.658
K2	Lunisolar semidiurnal	11.96	30.082
K1	Lunar diurnal	23.93	15.041
O1	Lunar diurnal	25.81	13.943
P1	Solar diurnal	24.06	14.958
Q1	Larger lunar elliptic diurnal	26.86	13.398
Mf	Lunisolar fortnightly	327.85	1.098
Mm	Lunar monthly	661.31	0.544

extreme wave amplitude resulted from the combination of two in-phase wave interactions. Furthermore, specific basin configuration may result in resonance. A simplified case, such as a rectangular basin, e.g., a lake, is commonly used to illustrate wave resonance. For instance, two waves traveling oppositely in a rectangular basin and perfectly reflected at each end have a resonance period (T_n) that is expressed as,

$$T_n = \frac{2L}{\sqrt{gh}} \tag{2.1}$$

where L is the length of basin and h is the depth of basin. Standing waves and resonance may also be produced in a basin with one open boundary that is forced harmonically. The resonant period of this case (T_{nf}) is expressed as,

$$T_{nf} = \frac{4L}{\sqrt{gh}} \tag{2.2}$$

The application of standing wave and resonance theory in realistic conditions are more complex due to non-uniform bathymetry and irregular coastal basins. The study area in this thesis is the Gulf of Maine, which is known for an extreme high tidal range inside the basin due to resonance (Garrett, 1972; Greenberg, 1987; Desplanque and Mossman, 2001).

2.3.3 Empirical equations for vertical velocity profile

In order to have a better comparison between model and observed data, velocity profiles were fitted to experimental data. The velocity profile, which can be obtained via measurements and/or 3-D ocean models, is a useful parameter for ocean studies. Many measurements have been conducted in effort to provide the vertical velocity profile in the ocean. However, the measurements are often not enough due to many factors, such as device specifications and maintenance.

Therefore, empirical methods were introduced to estimate the vertical current profile based on measured data. Power law is commonly used to give an estimate of velocity at specific water depth, which is expressed as

$$u(z) = u_{observed} \left(\frac{z}{d}\right)^{1/a} \tag{2.3}$$

where z is distance from seabed, d is total water depth and a is the profile coefficient. The value of a is set to 7 as recommended by previous research (Legrand, 2009; Peterson and Hennessey Jr, 1978).

2.3.4 Simulations of tidal turbine in ocean models

TEC energy extraction theoretically is based on the kinetic energy concept that is defined as energy that is produced by a body due to its motion, which is defined as,

$$E_k = \frac{1}{2} m u^2 \tag{2.4}$$

where E_k is the kinetic energy, m is the mass and u is the velocity. Current power is defined as the rate of change of current. Since mass flux can be expressed by volume flux times water density, kinetic power of a flow can be defined as,

$$P = \frac{dE_k}{dt} = \frac{1}{2} u^2 \frac{dm}{dt} \tag{2.5}$$

$$\frac{dm}{dt} = \rho \frac{d\mathbb{V}}{dt} = \rho Q = \rho A_t u \tag{2.6}$$

$$P = \frac{1}{2}\rho u^3 A_t \tag{2.7}$$

where P is power $(watt)$, t is time, V is the volume of water, ρ is the density of water, Q is flow rate (m^3/s), and A_t is the area of a turbine (m^2). From Equation 2.7, power is mainly dependent on the current velocity. The current power can also be expressed as power density,

$$P_{density} = \frac{\frac{1}{2}\rho A_t u^3}{A_t} \tag{2.8}$$

In Equation 2.7 and 2.8, the power is the available theoretical power in the ocean. Figure 2.2 displays the energy density for a range of current velocities. The curve shows that energy density rises significantly as current speed increases as it is proportional to u^3. However, the technical power, which is defined as estimated power generation by turbine, is significantly lower due to energy loss. Practical power, P_t, is estimated as,

$$P_t = C_p P \tag{2.9}$$

where C_p is the efficiency of TEC.

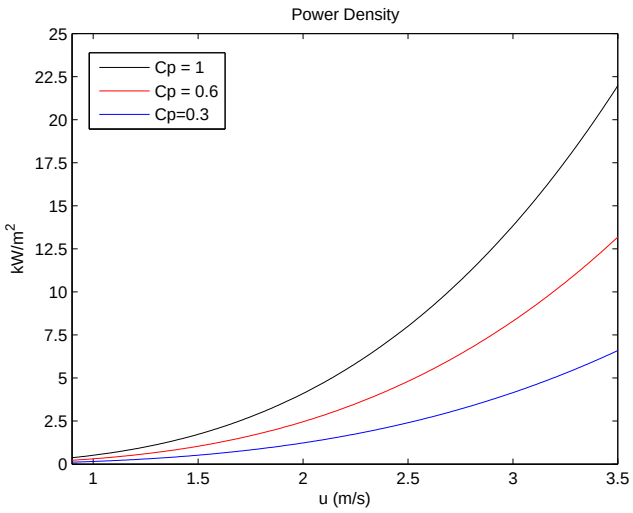

Figure 2.2. Current power curve (kW/m^2) at various current velocity (m/s).

2.4 Tidal modeling using ROMS

In this thesis, tidal simulations was done using Regional Ocean Modeling System (ROMS). The source code of ROMS is available online at www.myroms.org. This section gives the overview of the model.

2.4.1 ROMS theoretical background

ROMS is a three dimensional terrain following ocean model based on conservation of mass and momentum. ROMS solves the Reynolds-averaged Navier Stokes equations using the hydrostatic and Boussinesq assumptions (Hedström, 2012). Table 2.2 displays a list of symbols for ROMS formulation. ROMS numerical model solves the continuity equation,

$$\nabla.U = \frac{\partial u}{\partial x} + \frac{\partial v}{\partial y} + \frac{\partial w}{\partial z} = 0 \tag{2.10}$$

the horizontal momentum equations,

$$\frac{\partial u}{\partial t} + (U.\nabla)u = fv - \frac{\partial(\frac{p}{\rho})}{\partial x} - \frac{\partial}{\partial z}(\overline{u'w'} - v\frac{\partial u}{\partial z}) + S_u + D_u + F_u \tag{2.11}$$

$$\frac{\partial v}{\partial t} + (U.\nabla)v = fu - \frac{\partial(\frac{p}{\rho})}{\partial x} - \frac{\partial}{\partial z}(\overline{v'w'} - v\frac{\partial v}{\partial z}) + S_v + D_v + F_v \tag{2.12}$$

the vertical momentum equation with hydrostatic assumptions,

$$\frac{\partial(\frac{p}{\rho})}{\partial x} + \frac{p}{\rho_0}g = F_w \tag{2.13}$$

ROMS momentum equations include local and convective acceleration, Coriolis force, pressure, turbulent and fluid shear stresses, forcing terms and diffusive terms.

2.4.2 Bottom stress parameterization

At areas close to the ocean bed, many hydrodynamic parameters, such as velocity, shear stress, Reynolds stresses, energy dissipation, and turbulent viscosity

Table 2.2. List of Symbols in ROMS Formulation

Symbol	Description
x, y, z	cartesian direction coordinates
U	time averaged velocity vector (u, v, w)
f	coriolis parameter
p	pressure
ρ	density
u', v', w'	turbulent fluctuating velocities
S_u, S_v	horizontal tracer Sink/Source term
D_u, D_v	horizontal diffusive terms
F_u, F_v, F_w	forcing Terms
g	gravity
μ_t	turbulent eddy viscosity
τ_{bx}, τ_{by}	bottom stress
γ_1, γ_2	linear and quadratic bottom stress coefficient
s	sink/source terms of general length scale
C_p	turbine Efficiency coefficient
C_d	bottom drag coefficient
C_d^*	additional bottom drag coefficient

have a large gradient due to the no-slip condition at the seabed. ROMS applies bottom boundary layer theory with parameterized friction (Hedström, 2012). The method provides a force based on the drag force concept at the bottom boundary layer to represent the frictional mechanism. This formulation can be expressed as (see Table 2.2 for definition of parameters),

$$\tau_{bx} = (\gamma_1 + \gamma_2\sqrt{u^2 + v^2})u \tag{2.14}$$

$$\tau_{by} = (\gamma_1 + \gamma_2\sqrt{u^2 + v^2})v \tag{2.15}$$

$$\mu_t \left.\frac{\partial u}{\partial s}\right|_{s=-1} = \tau_{bx} \tag{2.16}$$

$$\mu_t \left.\frac{\partial v}{\partial s}\right|_{s=-1} = \tau_{by} \tag{2.17}$$

For tidal simulation, common values for bottom drag coefficient are 0.0025 to 0.0040. The value is usually adjusted according to model validation.

2.5 Tidal turbines simulation in ROMS model

TEC implementation in ocean model has been studied in the past to predict future change in ocean dynamics. There are several methods such as bottom friction method in 2-D momentum equation (Karsten et al., 2008; Garrett and Cummins, 2005; Sutherland et al., 2007), quadratic Rayleigh friction (Hasegawa et al., 2011), and 3-D actuator disc concept (Roc et al., 2013).

2.5.1 Increasing bottom friction to simulate energy extraction

The extracted power over a cross-sectional area can be theoretically treated as additional dissipation of energy due to bottom friction (Karsten et al., 2008; Garrett and Cummins, 2005; Sutherland et al., 2007). Using this concept, the bottom friction coefficient could be modified to simulate the far-field effect of TEC in the flow field. Table 2.3 shows the list of variables for TEC simulation in ROMS model. Total extracted power over a cross-sectional area is expressed as,

$$P_{ext} = \frac{P_t}{C_p} = 0.5N\rho A_t u^3 \tag{2.18}$$

In Equation 2.18, the extracted power is assumed ideal that all of the energy of the flow passing a TEC will be lost due to extraction and dissipation. The stress due to friction at seabed is formulated as,

$$\tau = \rho C_d |u| u \tag{2.19}$$

Equation 2.19 shows that stress at seabed is proportional to C_d. The friction force and dissipated power over a horizontal numerical cell area are formulated as,

$$F_{fric} = \tau A_{cell} \tag{2.20}$$

$$P_{diss} = F_{fric} u \tag{2.21}$$

Dissipated power also can be expressed as,

$$P_{diss} = \rho C_d |u| u^2 A_{cell} \tag{2.22}$$

The total extracted power by TEC is equivalent to the dissipated power by friction. Therefore, the additional power dissipation due to TEC can be simulated by the bottom drag coefficient. The formulation for TEC representation, as increased bottom drag coefficient, is casted by assuming that total extracted power (Equation 2.18) and dissipated power (Equation 2.22) by additional friction are the same. All of the variables from Equation 2.18 and Equation 2.22 will be canceled out except A_t, A_{cell}, N and C_d. Thus, the additional bottom drag coefficient can be formulated as,

$$C_d^* = \frac{C_p N A_t}{2 A_{cell}} \tag{2.23}$$

and the total bottom friction is expressed as,

$$C_d^{**} = (C_d + C_d^*) \tag{2.24}$$

Table 2.3. List of variables for turbine simulation in ROMS model.

P_{ext}	total extracted power	A_t	individual TEC blade area (m^2)
P_t	practical total extracted power	C_d	bottom drag coefficient
C_p	TEC efficiency	C_d^*	additional bottom drag coefficient
N	number of turbines in a numerical cell area	C_d^{**}	total bottom drag coefficient
A_{cell}	numerical cell area in ROMS model (m^2)	P_{diss}	dissipated power over a numerical cell area
F_{firc}	friction force	u	current velocity (m/s)

2.5.2 Actuator disc concept

Energy at TECs are generated by the torque which is applied to the rotor and is induced by movement of the blades. Consequently, wake and turbulence are produced at the area where a TEC operates (Pham and Martin, 2009). Recently, Roc , 2013 provided a method to incorporate wake due to stream turbine energy

extraction in regional ocean model as an assessment tool for turbine array optimization. In the cited study, actuator disc concept were implemented into ROMS. The modified ROMS momentum equation is expressed as (see Table 2.2 for list of variables),

$$\frac{\partial u}{\partial t} + (U.\nabla)u = fv - \frac{\partial(\frac{p}{\rho_0})}{\partial x} - \frac{\partial}{\partial z}(\overline{u'w'} - v\frac{\partial u}{\partial z}) + \vec{F}_t \tag{2.25}$$

In Equation 2.25, TECs are represented by $\vec{F}_t$, which is the force produced by TECs during power generation. The formulation of $\vec{F}_t$ is expressed as,

$$\vec{F}_t = -\frac{1}{2}\rho A_t C_p |u_\infty| u_\infty \vec{n} \tag{2.26}$$

where $|u_\infty|$ is current velocity at a location far from the turbine and $\vec{n}$ is the normal vector with respect to current velocity. The numerical implementation of TEC in ROMS is done with sub-grids between the ocean model and TEC. Figure 2.3 shows grid illustrations for TEC simulation in the cited study.

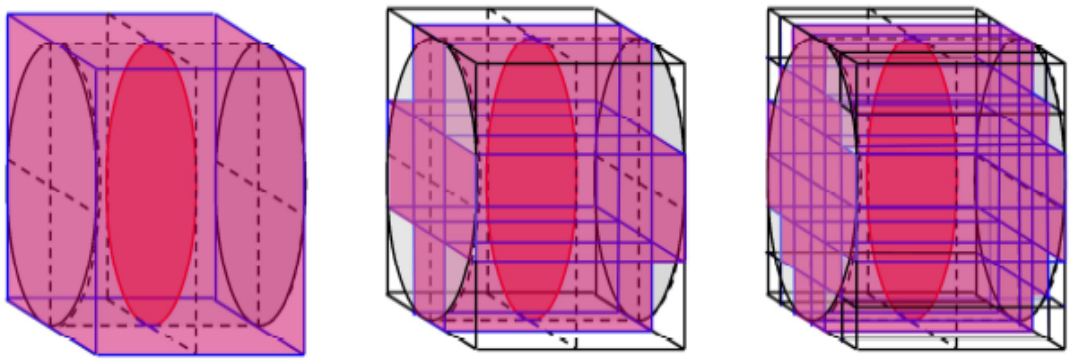

Figure 2.3. Grid illustrations for TEC simulation in ROMS using actuator disc concept. Black lines show ROMS ocean grid and blue lines represent the turbine grid in ROMS. Red shades represent turbine area in the grid. Picture from Roc, 2010.

2.6 ROMS tidal model development

The ROMS model domain was discretized with 1 arc-minute horizontal resolution, and 11 layers in a terrain-following vertical coordinate provided by ROM-

SAGRIF MATLAB toolbox (www.romsagrif.org). Model bathymetry was built using combined USGS bathymetric and NOAA Coastal Relief Model. The open boundary was forced by tidal water elevation and tidal velocity. Tidal forcing is provided by TPXO7 global tidal data set (volkov.oce.orst.edu/tides/) for 10 tidal constituents (M2, S2, N2, K2, K1, O1, P1, Q1, Mr, MM). Quadratic bottom friction was set to 0.003 for the entire domain for existing scenario. As the study focused on tidal dynamics in the Gulf Maine, some coastal areas with a lot of small islands such as Passamaquoddy-Cobscook Bay and Kennebec River estuary are excluded from computational domain. The model was run for a period of 30 days to capture spring-neap cycle.

In this thesis, 3 ROMS scenarios were assumed to examine the change in tidal dynamics:

- Tidal simulation at present condition.
- SLR scenario: +1 m change in bathymetry and boundary effect. Water elevation increase was assumed uniform and water do not flood coastal area.
- Energy extraction scenario combined with SLR scenario.

2.6.1 Tidal stream resource assesment

Quantifying the available resources is the first step for a tidal energy development. The dynamics of tides was modeled using ROMS (Regional Ocean Modeling System) followed by model validation to assure the accuracy of the results. Then, tidal-stream velocity was characterized at potential sites and was used to evaluate tidal energy. The effects of SLR on the tidal-stream energy resource was also examined in this part.

2.6.2 Impact of tidal stream turbines and SLR

Energy extraction using TEC may change the dynamics of tides in the Gulf of Maine. Therefore, the assessment of future tidal dynamics due to TEC is important to provide a better understanding of tidal energy extraction. In this study, the impact assessment of tidal-stream turbines and SLR was performed as previous research (Karsten et. al., 2008; Hasegawa et. al, 2011; Pelling and Mattias Green, 2013). The change in the dynamics of tide was first examined using a hypothetical scenario at Minas Passage, which is approximated with the added bottom friction method. Then, the impact of SLR and/or tidal energy extraction on the dynamics of tides in the Gulf of Maine was investigated.

CHAPTER 3

Results

3.1 Model validation

To determine model performance, a reference tidal simulation in the Gulf of Maine was set up using ROMS. A comparison between model results and observational data was performed to validate the model. Error calculation was done using root mean square error (RMSE) and scatter index (SI), which can be expressed as,

$$RMSE = \sqrt{\frac{(X^{obsv} - X^{ROMS})^2}{N^{data}}} \tag{3.1}$$

$$SI = \frac{RMSE}{\overline{x^{obsv}}} \tag{3.2}$$

where X^{ROMS} is ROMS results, X^{obsv} is observation data, and N^{data} is the total number of data. Tidal elevation on the Gulf of Maine was first validated with tidal water level measurement from stations available in the area and followed by tidal amplitude comparison for 11 tidal stations; then the validation for current was performed at 4 NERACOOS buoy locations. The period for model validation was selected on January-February 2011 due to data availability.

3.1.1 Tidal amplitudes validation

Tidal amplitude validation was first performed by time series comparison between model and observed data. Figure 3.1 shows comparison at Boston, Eastport, and Chatham tidal stations between model and observed data. The 3 locations was selected in the Gulf of Maine. Based on the plot, simulated tidal amplitude and phase agree very well with the observed data.

Further, tidal analysis was performed to obtain the amplitude and phase of M2 and S2 tidal components at tidal stations (see Figure 1.1 for the locations

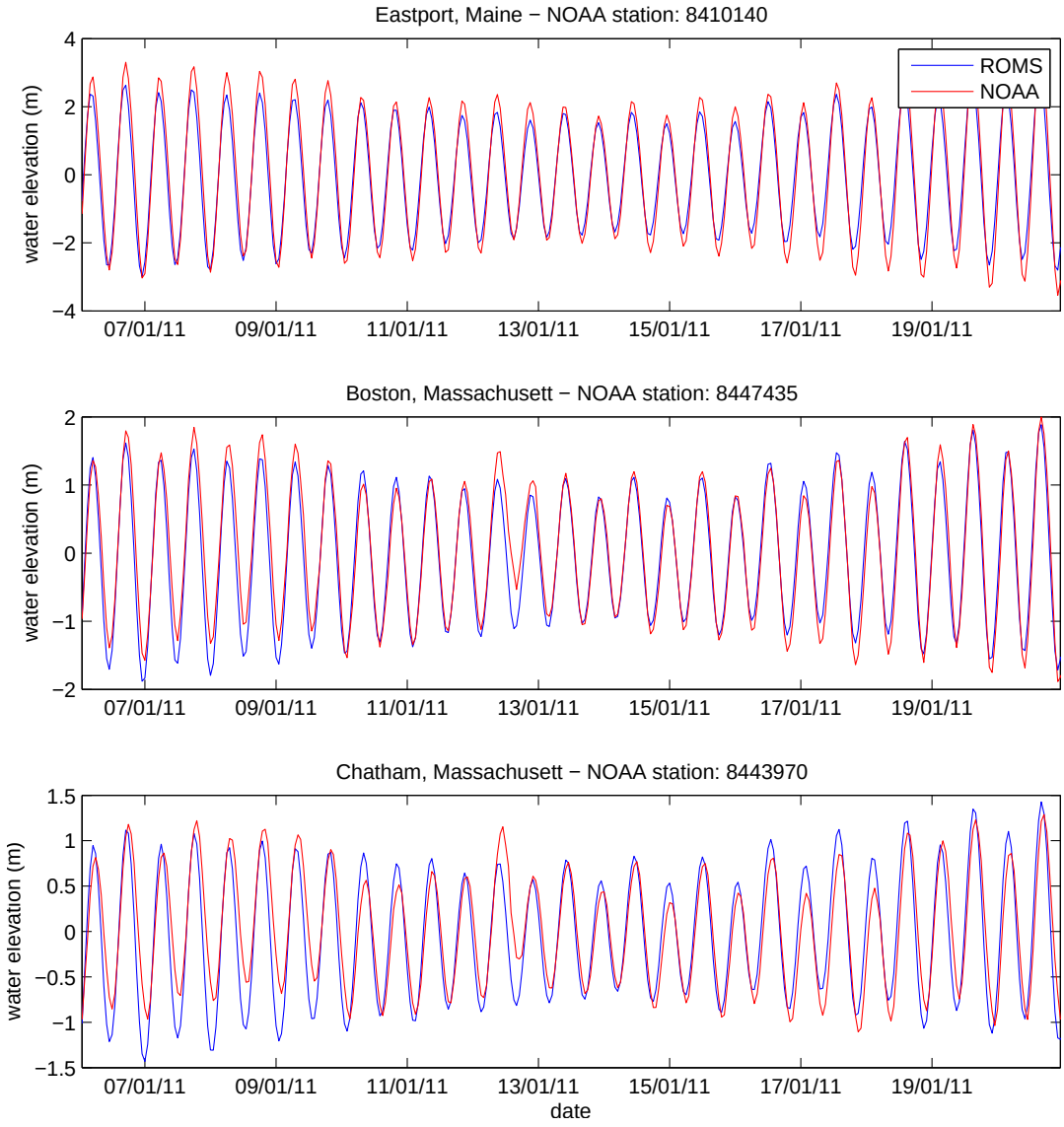

Figure 3.1. Water elevation time series comparison for Eastport and Boston.

of tidal stations). Due to data availability, 11 tidal stations and 5 tidal stations for M2 and S2, respectively, was used in model validation. Figure 3.2 shows the validation chart for both M2 and S2 components. Based on the results, RMSE for the amplitude and the phase of the M2 constituent are 7% and 9%, which was very convincing. For the S2 component, the comparisons were resulted in also a good agreement, the error was 19% and 9% for amplitude and phase. More details

are provided in Table 3.1 and 3.2 for the M2 and S2 components, respectively.

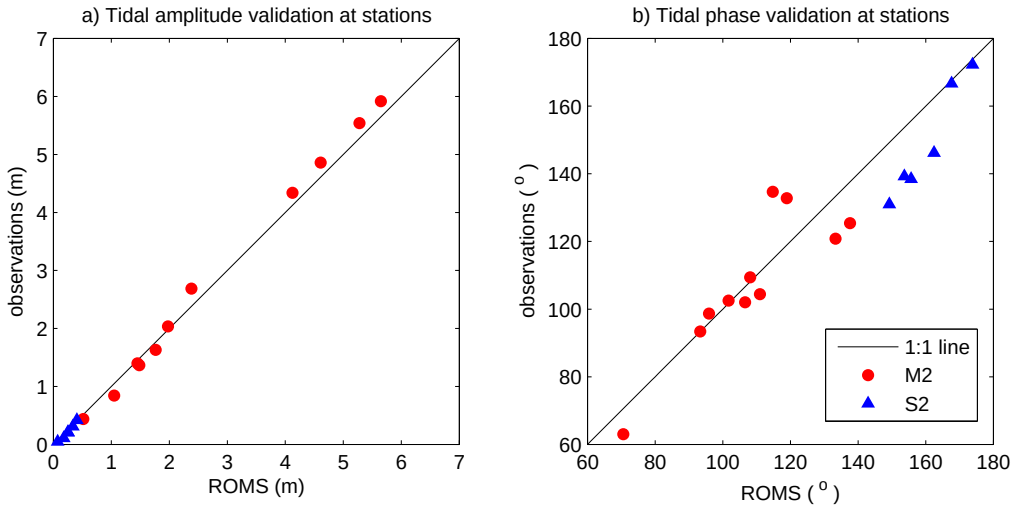

Figure 3.2. M2 and S2 validation at observation stations.

Table 3.1. Comparison of M2 constituents at 11 tidal stations

M2 observations	Observation		ROMS		Error	
	amplitude (m)	phase (^{o})	amplitude (m)	phase (^{o})	amplitude (m)	phase (^{o})
Portland	1.37	102.5	1.48	101.73	0.12	0.77
Eastport	2.69	98.7	2.38	95.92	0.31	2.78
Nantucket	0.44	134.7	0.52	114.78	0.08	19.92
Boston	1.40	109.4	1.45	108.11	0.05	1.29
Chatham	0.84	132.8	1.05	118.93	0.21	13.87
Cutler Farris	2.03	93.4	1.98	93.36	0.06	0.04
Yarmouth	1.63	63	1.77	70.59	0.14	7.59
Grindstone	4.86	104.4	4.61	110.98	0.25	6.58
Advocate Harbor	4.34	102	4.13	106.59	0.21	4.59
Minas Basin	5.54	120.8	5.28	133.34	0.26	12.54
Economy	5.92	125.4	5.65	137.63	0.27	12.23
				RMSE	0.198	9.7
				SI	7%	9%

Further model performance testing was also carried out using co-tidal maps, which provide a comprehensive assessment over the entire domain. The M2, S2, and M4 components were plotted to better assess the model performance. M2 and S2 were selected because they have significantly larger amplitude compared to other constituents in the Gulf of Maine. In addition, the M4 component was examined to determine nonlinear shallow water tide generation in the domain.

Table 3.2. Comparison of S2 constituents at 5 tidal stations

S2 observations	Observation		ROMS		Error	
	amplitude (m)	phase (^{o})	amplitude (m)	phase (^{o})	amplitude (m)	phase (^{o})
Portland	0.206	138.5	0.255	155.663	0.049	17.163
Eastport	0.420	139.3	0.407	153.667	0.013	14.367
Nantucket	0.047	166.7	0.073	167.647	0.026	0.947
Boston	0.213	146.2	0.251	162.446	0.038	16.246
Chatham	0.109	172.3	0.180	173.836	0.071	1.536
Cutler Farris	0.309	131.0	0.337	149.236	0.028	18.236
				RMSE	0.042	13.5
				SI	19%	9%

The M4 component also shows tidal asymmetry, which is caused by topographic features and friction at the seabed (Neill et al., 2014). The computed co-tidal for M2, S2 and M4 are shown in Figure 3.3, 3.5, and 3.6. Additionally, zoomed preview at the Bay of fundy for M2 and S2 are shown in Figure 3.7. From

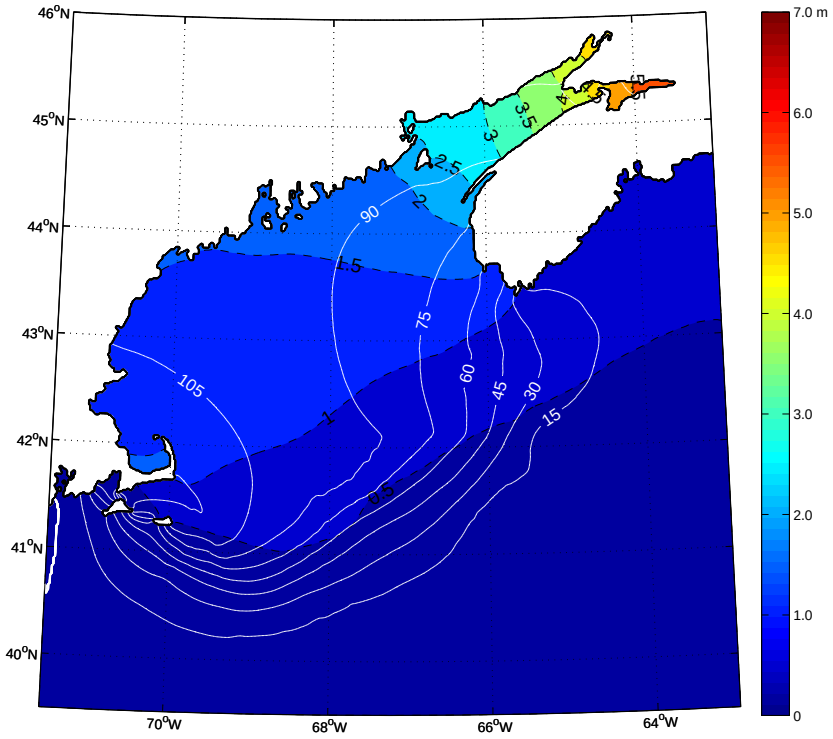

Figure 3.3. M2 co-tidal chart simulated using ROMS. Colorbar shows the amplitudes and white lines represent the phase.

the plot, M2 amplitudes are increasing from the continental shelf of the Gulf of Maine to the Bay of Fundy. The amplitudes are significantly higher in the Bay of

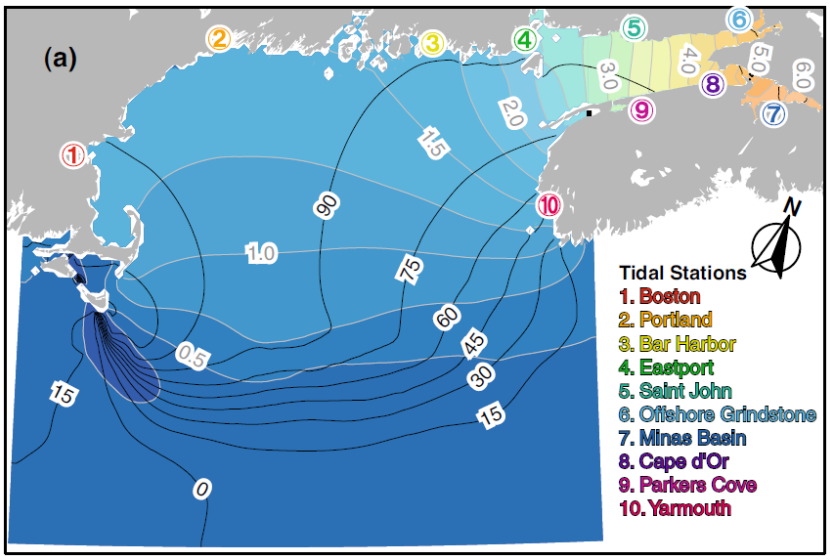

Figure 3.4. M2 co-tidal chart simulated using POM (Hasegawa et al., 2011). Colorbar shows the amplitudes (m) and black lines represent the phase (^{o}).

Fundy compared to the other regions in the Gulf of Maine due to resonance. For instance, Massachusetts shoreline and George's Bank are experiencing 1 m M2 tidal amplitude whereas areas inside the Bay of Fundy are having a significantly higher tide, more than 6 m. In addition, the plotted M2 co-tidal chart showing a very good agreement with the previous study by Hasegawa in 2011 using the Princeton Ocean Model (POM)(Figure 3.4) . In the cited study by Hasegawa, the 3-D model was built with nested grids, a ∼4.5 km resolution parent grid on the continental shelf and a ∼1.5 km sub-grid in the Bay of Fundy, and the open boundary was forced by five tidal constituents (M2, N2, S2, K1 and O1). Similarly, the S2 and M4 components show an increasing trend in amplitude from the continental shelf to the Bay of Fundy. The S2 amplitude starts at 0.1 m at the continental shelf and rises up to up to 1 m in the Bay of Fundy. For the M4 component, the amplitude is negligible on the continental shelf and is significantly higher in Minas Basin. ROMS predicted up to 0.5 m M4 amplitude in the Bay of Fundy. Based on the results, the model performed very well to simulate tidal amplitudes in the Gulf of

Maine.

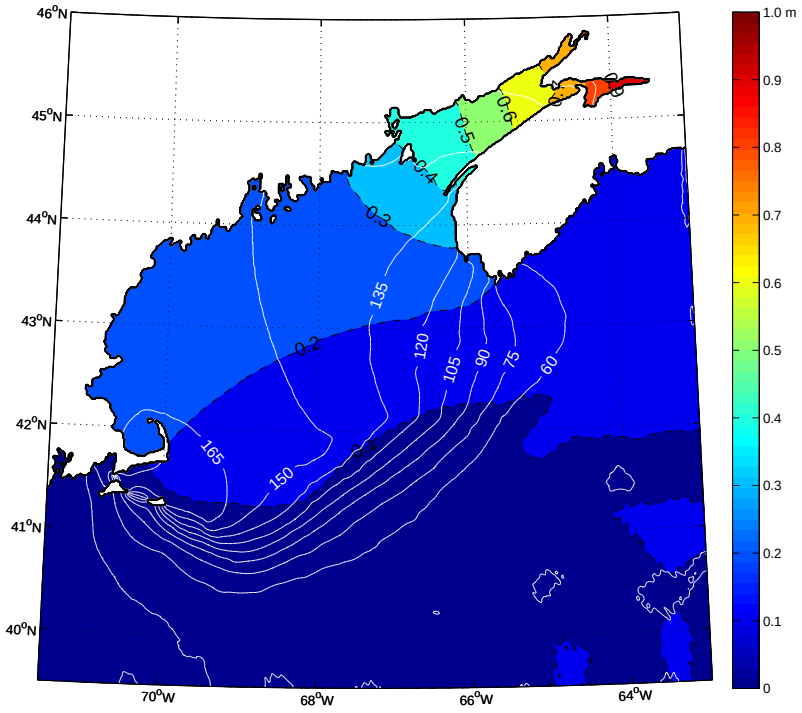

Figure 3.5. S2 co-tidal chart simulated using ROMS. Colorbar shows the amplitudes and white lines represent the phase.

3.1.2 Tidal current validation

Following the tidal amplitude and phase validation, tidal current was validation also performed by comparison with available velocity data. Time series of current velocity, tidal velocity components, and tidal ellipses were employed to validate the model.

Current observation data were retrieved from The Northeastern Regional Association of Coastal Ocean Observing Systems historical data (hrefwww.neracoos.org/www.neracoos.org) at four locations, N01, M01. B01, and E01 (see Figure 1.1). The dataset provides current velocity measurement at several depth locations such as 2 m, 10 m, 50 m and 250 m. In this thesis, power law was used to estimate current velocity profile based on measurement at 50 m. Observed

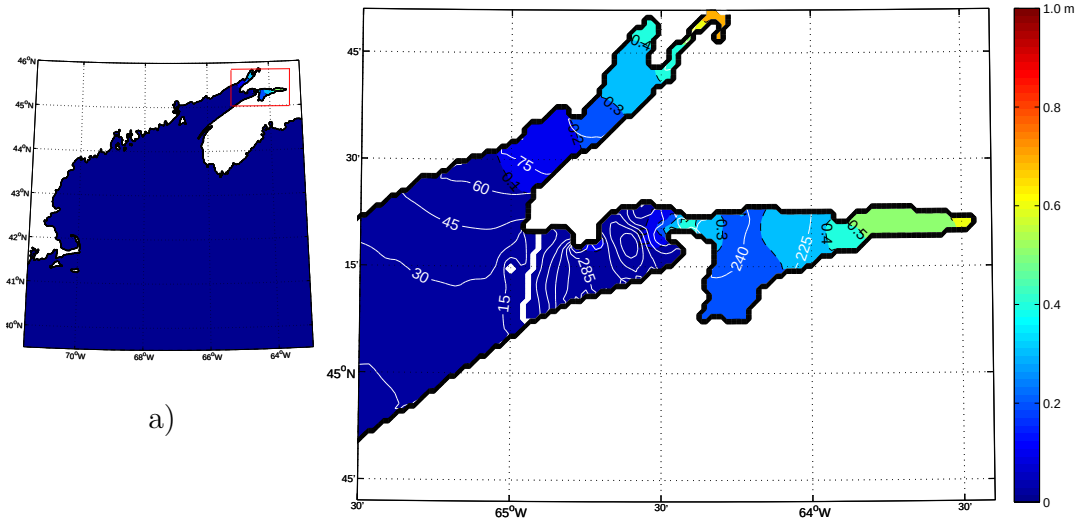

Figure 3.6. M4 co-tidal chart simulated using ROMS. a) the Gulf of Maine map. b) Zoomed view of the Bay of Fundy. Colorbar shows the amplitudes and white lines represent the phase.

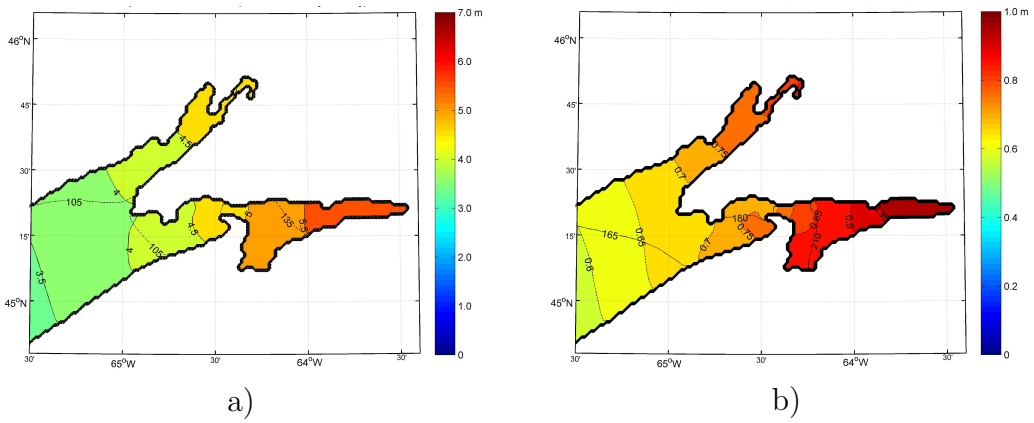

Figure 3.7. Zoomed cotidal map of M2 and S2. a) M2 component; b) S2 component. Colorbar shows the amplitudes and lines represent the phase.

and simulated depth-averaged current is shown in Figure 3.8. According to time series comparison, the predicted tidal-stream profile qualitatively showed acceptable results in terms of current velocity magnitude. However, observed data showed irregular peaks which indicates measured currents velocity are not only tidal related, but are also affected by other ocean currents (e.g.,wind generated current). To fur-

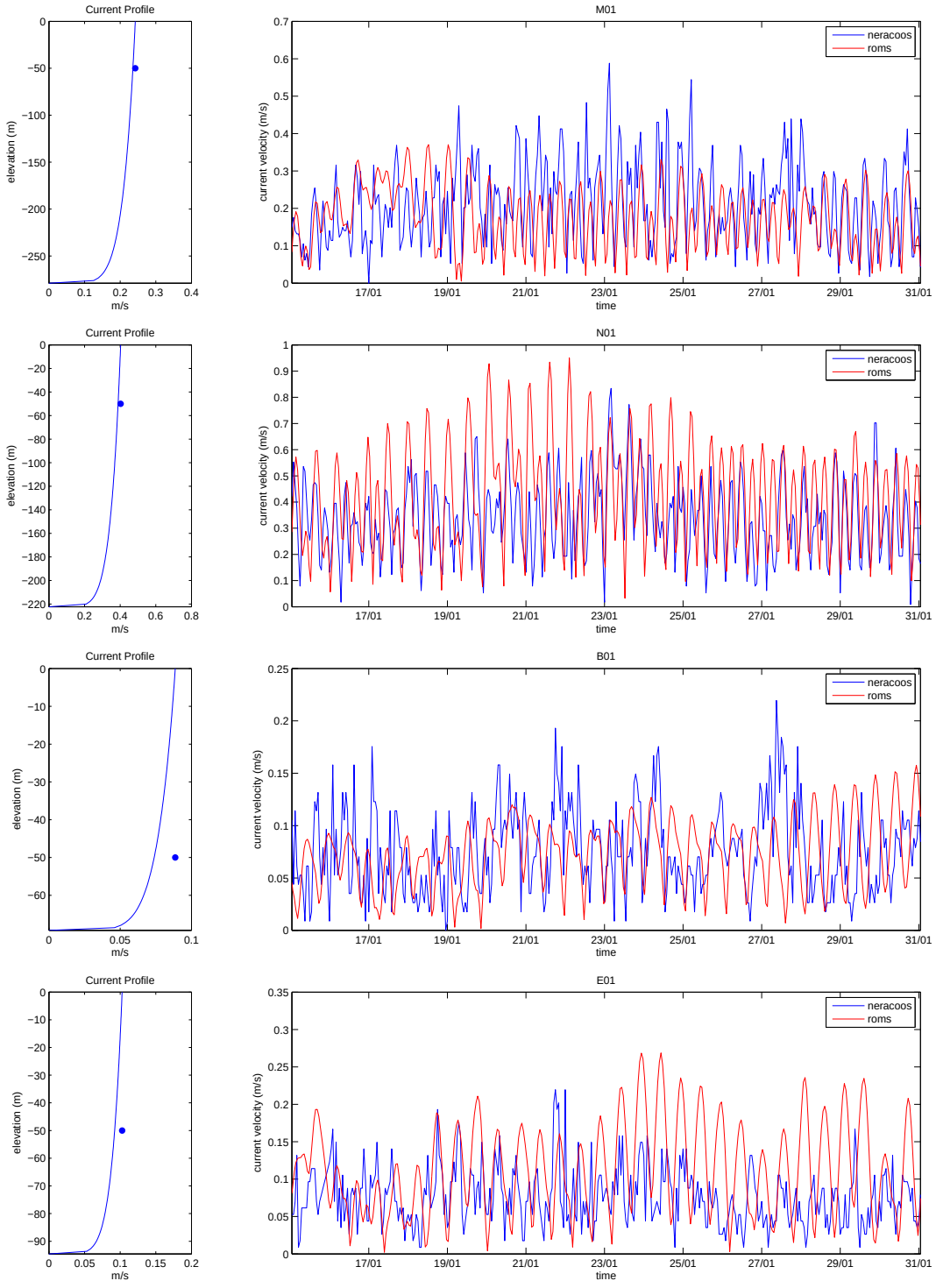

Figure 3.8. Comparison of model results and NERACOOS buoys: N01; M01; E01; and B01 (see Figure 1.1 for buoy locations).

ther examine the tidal-stream characteristic, a tidal analysis was done for the M2 tidal component using t_tide MATLAB toolbox (Pawlowicz et al., 2002). From the results, the simulated tides showed good agreement with buoy data, which is visualized in Figure 3.9. Ellipse shapes between buoys were qualitatively similar with small errors in inclination angle, minor axis and major axis. For instance, at N01 station, maximum current velocity was calculated at 0.85 m/s and 1.1 m/s for observed and ROMS results, respectively. Other locations, B01 and E01, also showed good agreement between model results and observations. In general, the model overestimated tidal currents velocity in the area. A noticeable error was found at buoy M01, which showed significant error at minor axis prediction. More details are provided in Table 3.3. Based on the tidal analysis results, simulated depth-averaged tidal currents is not agreed very well with observation data. Major axis comparison shows that ROMS overestimate the current velocity in the domain, SI calculated at 36%. The inclination angle between data show good results with 6% error. A noticeable error was found at the minor axis with 120% scatter index between observation and model.

Table 3.3. Tidal ellipse parameters comparison between ROMS and observed data.

Buoy	NERACOOS data			ROMS output			Error		
	Major Axis (m)	Minor Axis (m)	Inclination (^{o})	Major Axis (m)	Minor Axis (m)	Inclination (^{o})	Major Axis (m)	Minor Axis (m)	Inclination (^{o})
N01	N01	0.429	-0.127	151.330	0.555	-0.153	140.574	0.126	0.026
M01	M01	0.211	-0.002	95.545	0.218	0.030	93.059	0.007	0.032
B01	B01	0.048	0.021	120.483	0.063	0.030	122.538	0.015	0.008
E01	E01	0.053	0.037	68.643	0.090	0.047	76.048	0.037	0.010
						RMSE	0.066	0.021	6.726
						SI	36%	-120%	6%

To further assess ROMS performance, the tidal ellipse chart for the Gulf of Maine was plotted and was compared to the previous study by Hasegawa et al. in 2011 (Figure 3.11) that is based on Princeton Ocean Model (POM). Figure 3.10 and 3.11 show that the tidal ellipses at the two studies visually matched very well. From the results, at an area close to the Bay of Fundy, the ellipse shapes

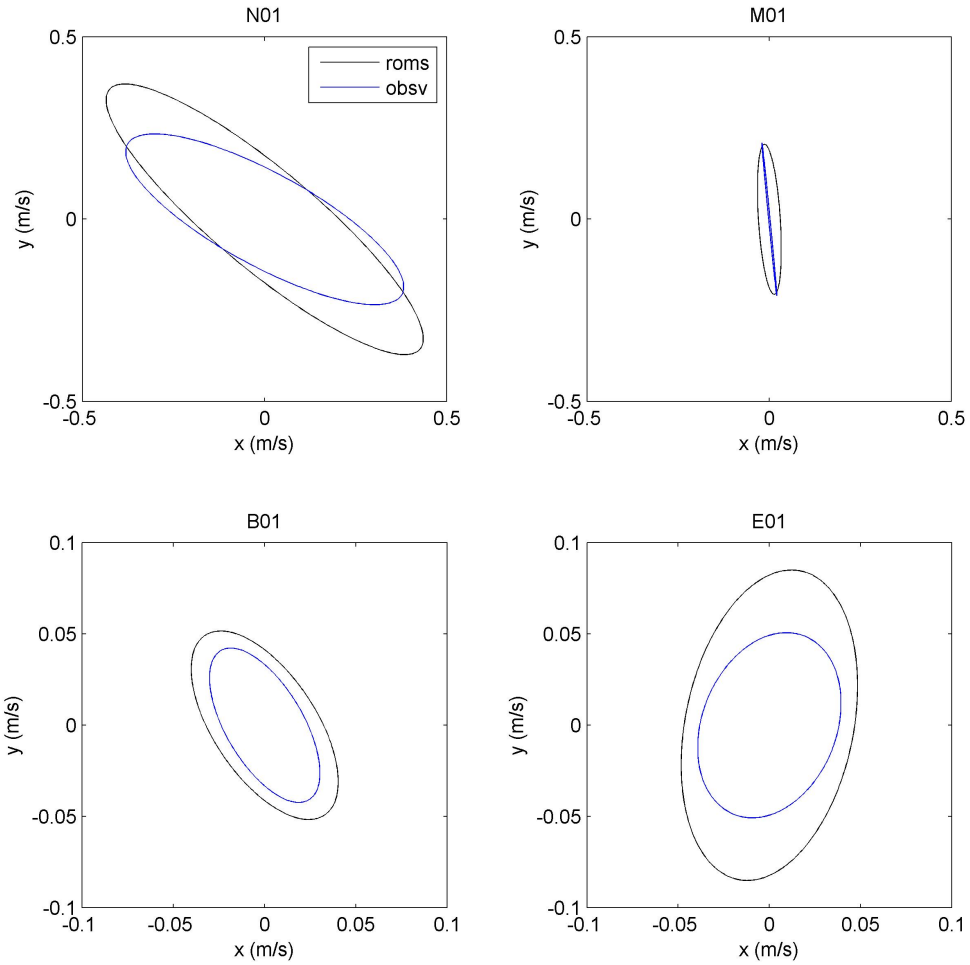

Figure 3.9. Comparison of tidal ellipses from model results and measurement locations.

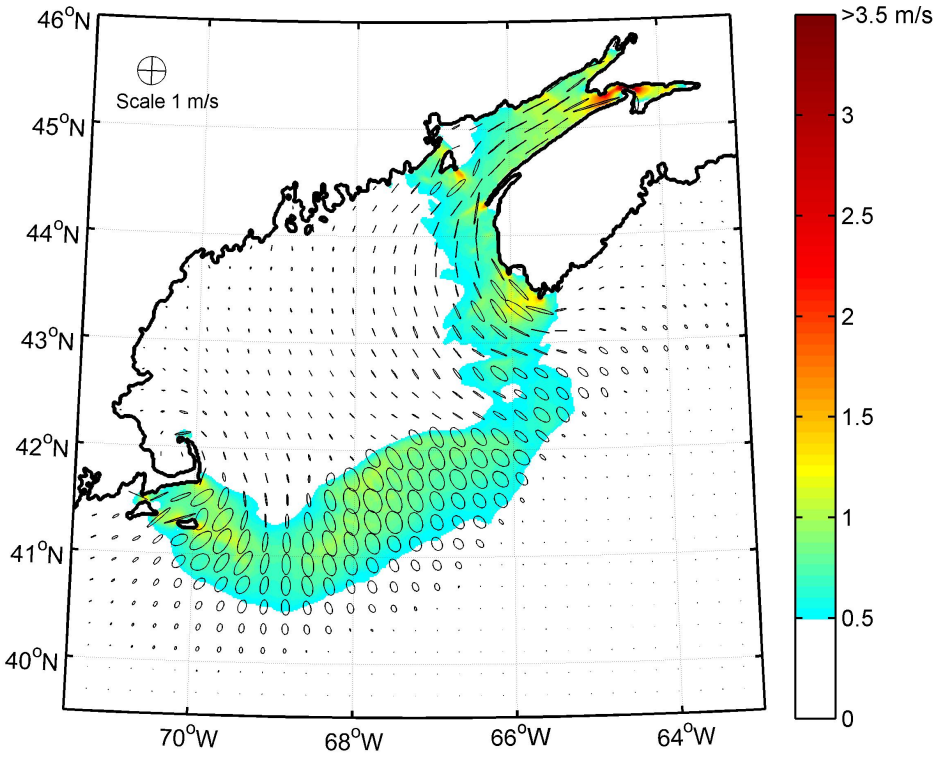

a)

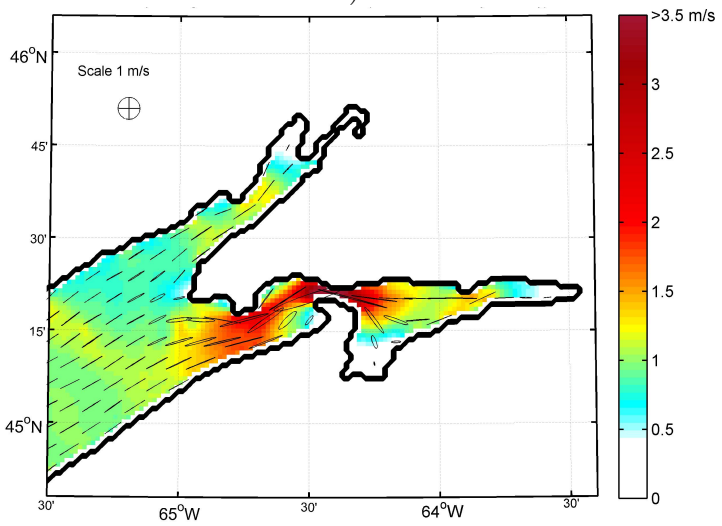

b)

Figure 3.10. a) M2 tidal ellipses diagram based on ROMS results; b) zoom preview for the Bay of Fundy area. Colorbar shows maximum tidal velocity for M2 component.

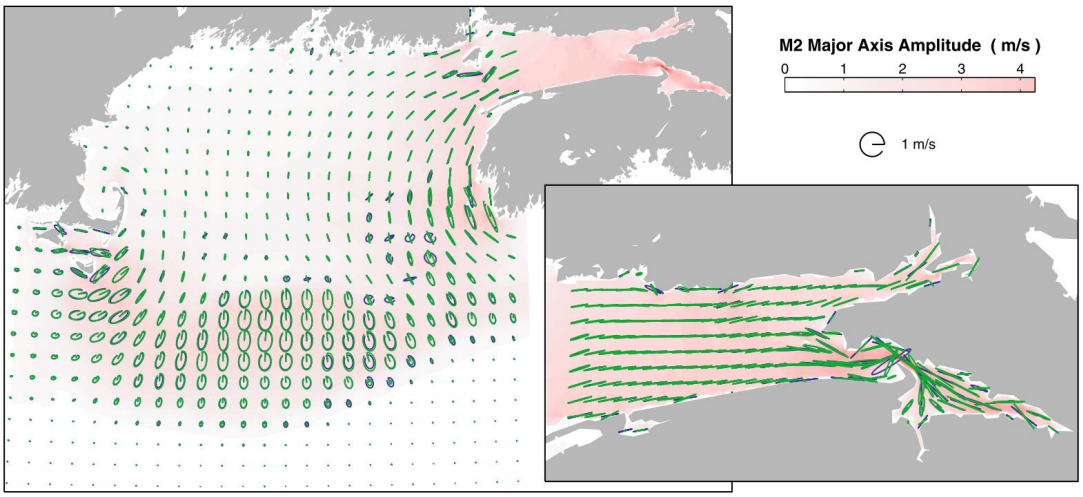

Figure 3.11. The Gulf of Maine M2 Depth-averaged tidal ellipses calculated using Princeton Ocean Model (POM). Picture is retrieved from study by Hasegawa in 2010. Green lines represent POM results and blue lines display Webtide tidal model which used for validation in the cited study (www.bio.gc.ca).

are significantly thinner and almost approach a rectilinear shape, indicating a unidirectional current field, which is preferred for a TEC development site. The model simulation resulted in a high tidal current velocity ($> 1.5\ m/s$) at several areas, such as, Nantucket, outer Gulf of Maine Area, Grand Manan Island, Western side of Nova Scotia, and Minas Passage. The highest simulated tidal current was predicted at Minas Passage, which was computed to be up to 4.5 m/s maximum velocity.

3.1.3 Increased bottom drag coefficient and tidal energy extraction

In this part, we set up an energy extraction scenario to test the increasing bottom drag coefficient method in ROMS. The extraction scenario was examined considering a suggested optimum configuration of array (Divett et al., 2013) to evaluate the spacing of TEC. Total horizontal area of the Passage is $\sim$10 km^2 which consists of six numerical cells (1287 m x 1287 m), as shown in Figure 3.12. Minas Passage is able to fit 300 TECs in total (12 by 25 units across and along

central axis of the water flow, respectively). TEC are assumed to be a horizontal axis and have a 20 m diameter. Also, TEC was assumed ideal, $C_p = 1$ The scenario was further simulated in the model using the increased bottom friction method, resulting in an 0.0047 additional bottom drag coefficient (C_d^*) and an 0.0077 total bottom friction (C_d^{**}). Table 3.4 shows the summary of the extraction scenario. Figure 3.13 illustrates TEC array on ROMS grid for the energy extraction scenario.

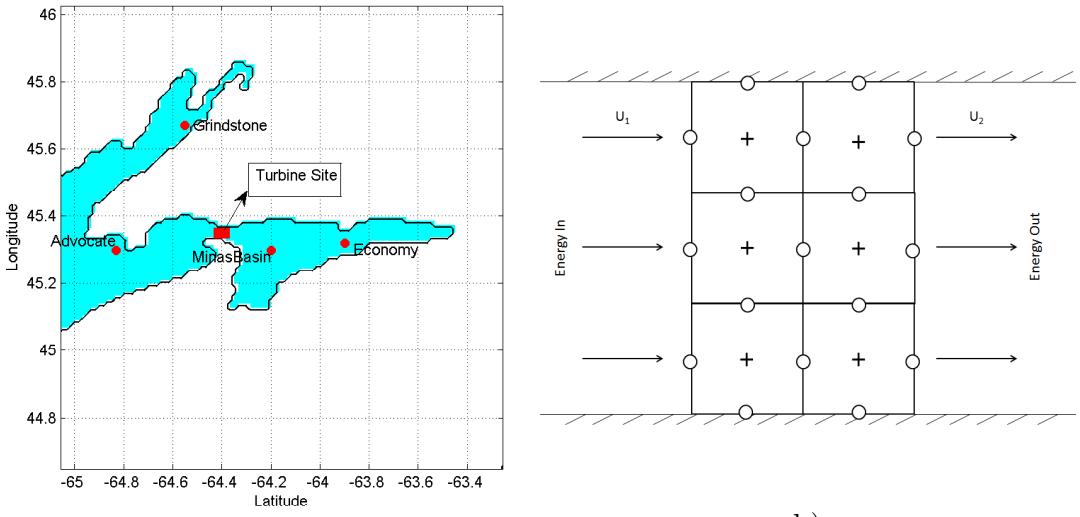

a) b)

Figure 3.12. a) Location of TEC site at Minas Passage. b) ROMS discretization for Minas Passage.

Table 3.4. Tidal energy extraction scenario summary

Cell size (m)	1287 x 1287
Number of cell	6; 3 in y direction and 2 in x direction
Total cell area A_{cell} (m^2)	9938214
Turbine configuration	7.5 D (across the flow field); 10 D (along the flow field)
Total number of turbines	300
Turbine diameter (m)	20
A_t (m^2)	94248
Average depth at Minas Passage (m)	54
C_d^*	0.0047
C_d^{**}	0.0077
P_{diss} (GW)	1.23

To test the increasing bottom friction method, we have computed the energy flux in Minas Passage to see if change in the flux equals energy extraction. Total

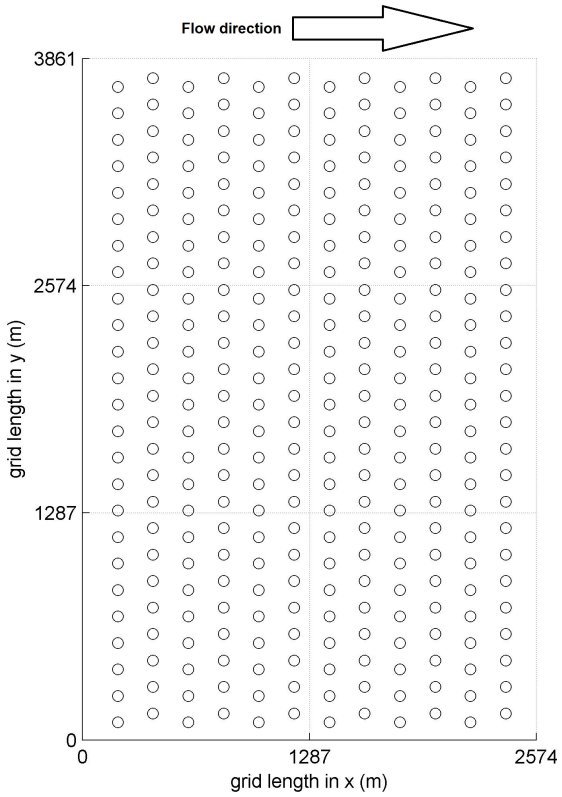

Figure 3.13. Illustration of TEC array on ROMS grid for 1.23 GW energy extraction scenario.

energy influx and outflux were calculated at 2.67 GW and 1.50 GW, respectively, which resulted in 1.18 GW of total dissipated energy. The calculated flux agreed well with the 1.23 GW tidal-stream energy extraction scenario. Table 3.5 shows the summary of the energy flux calculation.

Based on the results in this part, we were convinced that the increasing bottom drag coefficient method is applicable for TEC array representation in ROMS

3.2 Tidal resource assessment in the Gulf of Maine

In this section, we will focus on tidal-stream energy resources in the study area. ROMS model was run for a 30 days period, which is the suggested period to assess energy resource according to European Marine Energy Centre (www.emec.org.uk). Then, the average power density was evaluated over the entire domain based on

Table 3.5. Power flux calculation summary at Minas Passage for 1.23 GW tidal-stream extraction scenario

	In	Out
Average depth (m)	47.68	55.29
Crossectional Area (m^2)	184104.40	213492.04
Power / cross-sectional Area (kW/m^2)	14.27	6.30
Total energy (kW)	2673012.27	1495956.77
Total energy (GW)	2.67	1.50
Influx - Outflux (GW)		1.18
Energy extraction by turbines (GW)		1.23

the outputs. The impacts of SLR on the dynamics of tide were also examined to predict future tidal resource in the domain.

3.2.1 Present tidal energy resources in the Gulf of Maine

The tidal resource can be evaluated for both maximum theoretical power and average theoretical power. Maximum theoretical power may indicate a promising site, however, tidal current velocity and direction are changing over a tidal cycle and during spring-neap cycle. Thus, for tidal energy development, average tidal-stream energy resource also commonly used to represent the potential of a site. direction are changing over a tidal cycle and during spring-neap cycle.

First, the maximum spring velocity was used to estimate maximum theoretical power density in the area (Figure 3.14). In general, based on the results, 3 to 8 kW/m^2 maximum theoretical power is available in the study region, which is a relatively good resource. The highest power density was predicted at Minas passage, having up to 4.5 m/s current velocity which results in up to 23.24 kW/m^2 and 7.70 GW available maximum theoretical power. The results at Minas Passage agree with previous studies which estimated $\sim$7 GW available maximum theoretical power (Karsten et al., 2008; Hasegawa et al., 2011; Cornett et al., 2010; Pelling and Mattias Green, 2013), as shown in Table 3.6. Table 3.7 shows the summary of available maximum theoretical power in the domain.

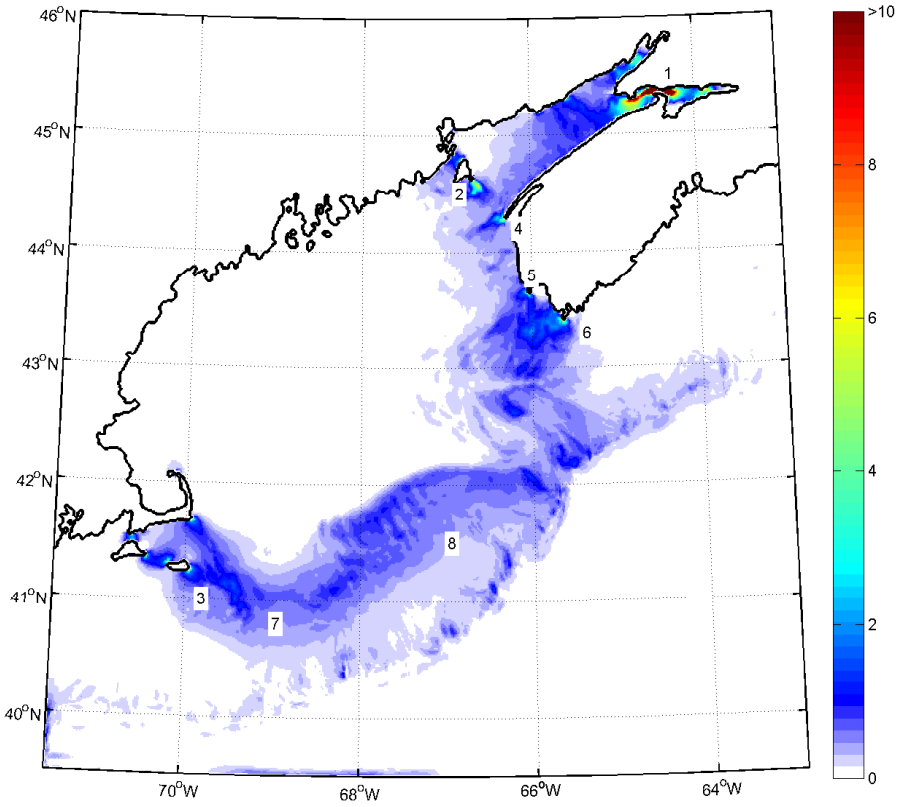

Figure 3.14. Maximum theoretical power density (kW/m^2) in the Gulf of Maine. Numbers show selected sites with high resources.

Table 3.6. Summary of available maximum theoretical power at Minas Passage and comparison with the previous studies.

	Units	Pelling (2013)	Cornett (2010)	Hasegawa (2011)	Karsten (2008)	ROMS
Maximum Available Power	GW	7.1	-	7.60	7.00	7.70
Max. Available Power per area	kW/m2	-	>24	22.82	22.03	23.24

Figure 3.15 shows the average power resources in the domain. In detail, the average tidal energy is between 0.5 to 2.0 kW/m^2 and potential sites were identified at Nantucket shoals, western side of Nova Scotia, and Grand Manan Island. In Minas Passage, the average power density is 14.27 kW/m^2. Based on the results, the highest for both maximum and average tidal energy resources are Minas Passage while other sites have significantly lower resources. However, many sites have sufficient velocity ranges as demonstration sites or small power generation

Table 3.7. Summary of available maximum theoretical power in the Gulf of Maine (see Figure 3.14 for site locations).

Maximum power density	
Location	Present (kW/m^2)
1. Minas Passage	23.24
2. Great Manan Island	3.75
3. Nantucket Shoals	2.52
4. Westport	4.46
5. Big Tusket Island	3.41
6. Shag Harbor	5.31
7. Great South Channel	0.67
8. Georges Bank	0.62

projects.

3.2.2 Impacts of SLR on the tidal stream energy resource

SLR will change the bathymetry and global dynamics of the tides and therefore modifies the tidal-stream energy resource. A recent study by Wilmes (2016) predicted a 10% change in the M2 amplitude along the boundary due to a 1 m SLR in the Gulf of Maine. In this part, we examine how the tidal resource in the Gulf of Maine will respond to SLR; the change in bathymetry and the dynamics of tides. Here, we set up two simulations:

1. +1 m uniform change in bathymetry.

2. +1 m uniform change in bathymetry and boundary effects (see Section 2.1.5 for details).

Figure 3.15 shows the average theoretical power and difference plot for the SLR scenarios and Table 3.8 show the summary of available average theoretical power and the impacts on the resources. Based on the results, the inclusion of SLR can significantly modify the resources. For instance, considering the impact just on the modified bathymetry scenario, tidal-stream energy resource in the domain generally increased between 0.2 - 0.5 kW/m^2 range excluding Minas Passage. Also, up to a 0.05 kW/m^2 decrease in the resource was predicted at Yarmouth and Shag

Harbour. At the passage, the resource increased significantly from 13 to 16.32 kW/m^2. By implementing the impact of SLR on the boundary, the energy resource increased between 0.05 to 0.15 kW/m^2. Compared to the first SLR scenario, 1.81 kW/m^2 rise in average tidal energy resource was predicted at Minas passage.

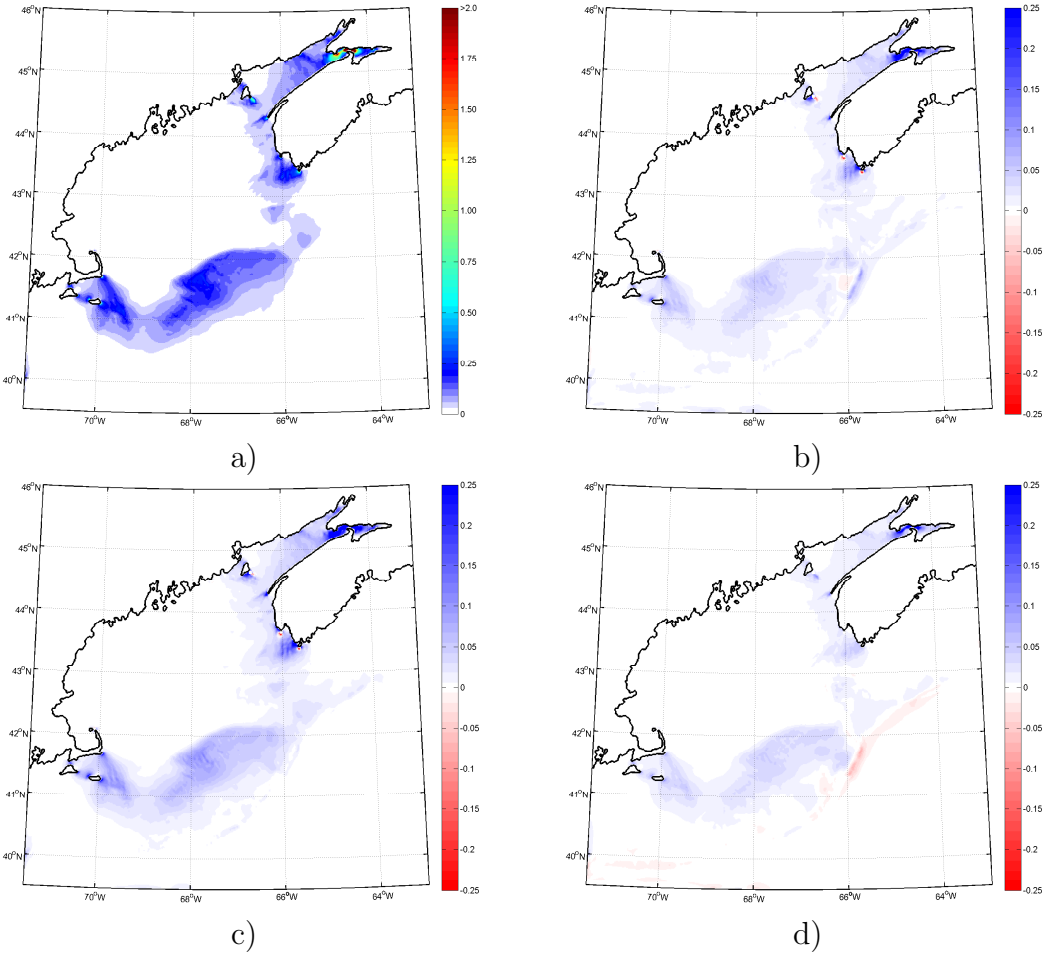

Figure 3.15. Impact of SLR on tidal-stream energy resources. a) Available average tidal-stream energy resources (kW/m^2); b) Changes in the resources due to +1 m modified bathymetry scenario (kW/m^2); c) Changes in the resources due to +1 m modified bathymetry scenario and the change in tides along the boundary (kW/m^2). d) Difference between b and c (kW/m^2).

3.3 Impacts of energy extraction and SLR on tidal dynamics

Tidal energy extraction in general affects ocean dynamics and may result in adverse physical and environmental impacts. In this part, we set up two simulation

Table 3.8. Summary of available average theoretical power and the impacts on the resources in the Gulf of Maine (see Figure 3.14 for site locations).

Average power density					
Location	Present (kW/m^2)	Differerence (kW/m^2)		Differerence (%)	
		+1 m bathymetry scenario	+1 m and +10% M2 amplitude scenario	+1 m bathymetry scenario	+1 m and +10% M2 amplitude scenario
1. Minas Passage	14.27	+ 3.32	+ 5.35	23%	37%
2. Great Manan Island	0.60	- 0.07	+ 0.00	-12%	0%
3. Nantucket Shoals	0.44	+ 0.15	+ 0.24	34%	55%
4. Westport	0.59	+ 0.25	+ 0.37	42%	63%
5. Big Tusket Island	0.57	- 0.42	- 0.41	-74%	-72%
6. Shag Harbor	0.85	- 0.37	- 0.32	-44%	-38%
7. Great South Channel	0.07	+ 0.01	+ 0.02	14%	29%
8. Georges Bank	0.24	+ 0.06	+0.11	25%	46%

Difference values are compared to average power at present

scenarios regarding energy extraction and SLR:

1. Energy extraction scenarios: 0.74 GW; 1.23 GW; and 2.5 GW. .

2. Energy extraction scenarios combined with +1 m SLR (including the changes in the boundary).

The energy extraction scenario was set based on the testing scenario for the increasing bottom drag coefficent, 1.23 GW, which have a total of 300 TEC in the array and C_p is assumed ideal. By using the increasing bottom friction method, additional bottom friction calculation (see Equation 2.23) is mostly dominated by C_p, A_t, and A_{cell}, thus, energy extraction scenario can be set up by adjusting those parameters. For 0.74 MW extraction scenario, the 1.23 GW extraction case was modified by the implementation of the betz limit, C_p is 0.6. The last extraction scenario, 2.5 GW was set up to match available estimated stream-energy in Minas Passage by FORCE. For the last scenario, the area of turbine blade was increased to extract 2.5 GW from water flow without modifying the total number of turbine and the turbine configuration. Further, we included SLR scenarios into energy extraction scenarios to predict future change in the dynamics of tide in the Gulf of Maine. Table 3.9 show the summary of energy extraction scenarios in this study.

All of the scenarios are located in $\sim$10 km^2 horizontal area in Minas Passage. Boston and Minas Basin (see Figure 3.16) was selected to be the focus area based on basin configuration. For instance, Minas Basin is located at the end of the basin, while Boston is one of sites in the farthest area from Minas Passage.

Table 3.9. Summary of energy extraction scenarios in ROMS.

Energy extraction scenario	Cp	Turbine diameter, D (m)	Total turbine area, A_t (m^2)	C_d^*	C_d^{**}
0.74 MW	0.60	20	94248	0.028	0.058
1.23 GW	1.00	36	305360	0.047	0.077
2.50 GW	0.60	62	905720	0.092	0.122

The impacts of energy extraction was first examined in terms of the change in the M2 component amplitude. In the Gulf of Maine, Greenberg, 1979 found that basin resonance period (12.8 hour) is very close to the period of M2 component (12.42 hour). According to the cited study, it was concluded that any change in the dynamics of tides in the domain will mostly affect M2 component. Thus, tidal analysis was done to obtain the amplitude of tidal components. Figure 3.17 and 3.18 shows the impacts of energy extraction scenario and the combined scenarios, respectively. From the results of extraction scenarios at present day (Figure 3.17), tidal amplitude will decrease in Minas Passage and will increase in Boston. In Minas Basin, the decrease in the M2 amplitude is growing significantly as energy extraction in Minas Passage is larger. For instance, at 740 MW energy extraction scenario, the decrease in the M2 amplitude was computed at -0.86%, which relatively very small. At 2.5 GW energy extraction scenario, -3.42% decrease in the amplitude was predicted, resulting in -0.179 m M2 tidal amplitude difference. Oppositely, the M2 amplitude on Massachusetts coastal area is rising in respect with energy extraction scenarios in Minas Passage. The maximum increase in the M2 tidal amplitude was produced by the 2.5 GW energy extraction scenario, 0.94 % in Boston, which is relatively very small compared to the present day M2 amplitude.

In general, the far field impacts of tidal energy extraction in Minas Passage on the M2 amplitude are relatively small in the region with less than 4% changes at the highest scenario in this study, considering 2.5 GW energy extraction. Further, the inclusion of SLR scenarios into the energy extraction scenarios alters the tidal dynamics for M2 component in the Gulf of Maine. The maximum changes in the M2 component rise to 7.83%, which is identified in Boston, resulting in 11 cm M2 tidal amplitude at 2.5 GW energy extraction scenario. In Minas Basin, the change in the M2 tidal amplitude is also changes into increase in the amplitude. From the results of the combined scenarios, it was concluded that the inclusion of SLR into energy extraction scenarios significantly alter the dynamics of tide in the Gulf of Maine. More details are shown in Table 3.10 for the impacts of energy extraction scenarios on the M2 tidal amplitude in Boston and Minas Passage.

Table 3.10. Impact of energy extraction and SLR scenarios on the M2 amplitude at Minas Basin and Boston. The M2 amplitudes at the present day are 5.24 m and 1.49 m for Minas Basin and Boston, respectively.

	Change in meter		Change in %	
Scenario	Minas Basin	Boston	Minas Basin	Boston
Energy extraction scenario:				
740 MW	-0.045	0.002	-0.86%	0.13%
1230 MW	-0.078	0.007	-1.49%	0.47%
2500 MW	-0.179	0.014	-3.42%	0.94%
SLR scenario:				
+1 m SLR and boundary effect	0.287	0.103	5.48%	6.94%
Energy extraction and SLR scenario				
740 MW and SLR	0.184	0.097	3.52%	6.54%
1230 MW and SLR	0.122	0.096	2.32%	6.46%
2500 MW and SLR	0.051	0.117	0.97%	7.83%

Changes are relative to the present day scenario

Additionally, we also computed the change in the tidal range to see the total changes in water elevation. Figure 3.19 and 3.18 show the change in the tidal range for energy extraction and the combined scenarios. Similar to the results for M2, the tidal range differences rise as energy extraction in Minas Passage is

higher. For instance the relative changes in Minas Basin is -0.79% at 740 MW energy extraction scenario and -3.59% at 2.5 GW energy extraction scenario. The inclusion of SLR scenario into the simulation also shows similar qualitative trend with the M2 tidal amplitude analysis because the resonance in the Gulf of Maine is determined by the M2 component. Table 3.11 shows more details for the impacts of energy extraction scenarios on the tidal range in Boston and Minas Passage. Table 3.12 shows summary of the model validation from previous research related to the impacts of tidal energy extraction in the Gulf of Maine.

Table 3.11. Impact of energy extraction and SLR scenarios on the tidal range at Minas Basin and Boston. The tidal range at the present day are 15.08 m and 4.54 m for Minas Basin and Boston, respectively.

	Change in meter		Change in %	
Scenario	Minas Basin	Boston	Minas Basin	Boston
Energy extraction scenario:				
740 MW	-0.109	0.038	-0.73%	0.85%
1230 MW	-0.283	0.026	-1.88%	0.59%
2500 MW	-0.541	0.074	-3.59%	1.65%
SLR scenario:				
+1 m SLR and boundary effect	0.440	0.191	2.92%	4.20%
Energy extraction and SLR scenario				
740 MW and SLR	0.204	0.199	1.35%	4.39%
1230 MW and SLR	0.003	0.194	0.02%	4.28%
2500 MW and SLR	-0.224	0.247	-1.48%	5.43%

Changes are relative to the present day scenario

Table 3.12. Summary of the model validation from research related to the impacts of tidal-stream energy extraction in the Gulf of Maine.

Research	Model	Error formulation	Amplitude	Phase
Karsten, 2008	FVCOM	Not stated	-	-
Cornett, 2010	TELEMAC-3D	Based on time series comparison qualitatively without error calculation	-	-
Hasegawa, 2011	POM	Averaged relative amplitude errors	3.1%	2.7%
Pelling and Green, 2013	OTIS	Not stated	-	-

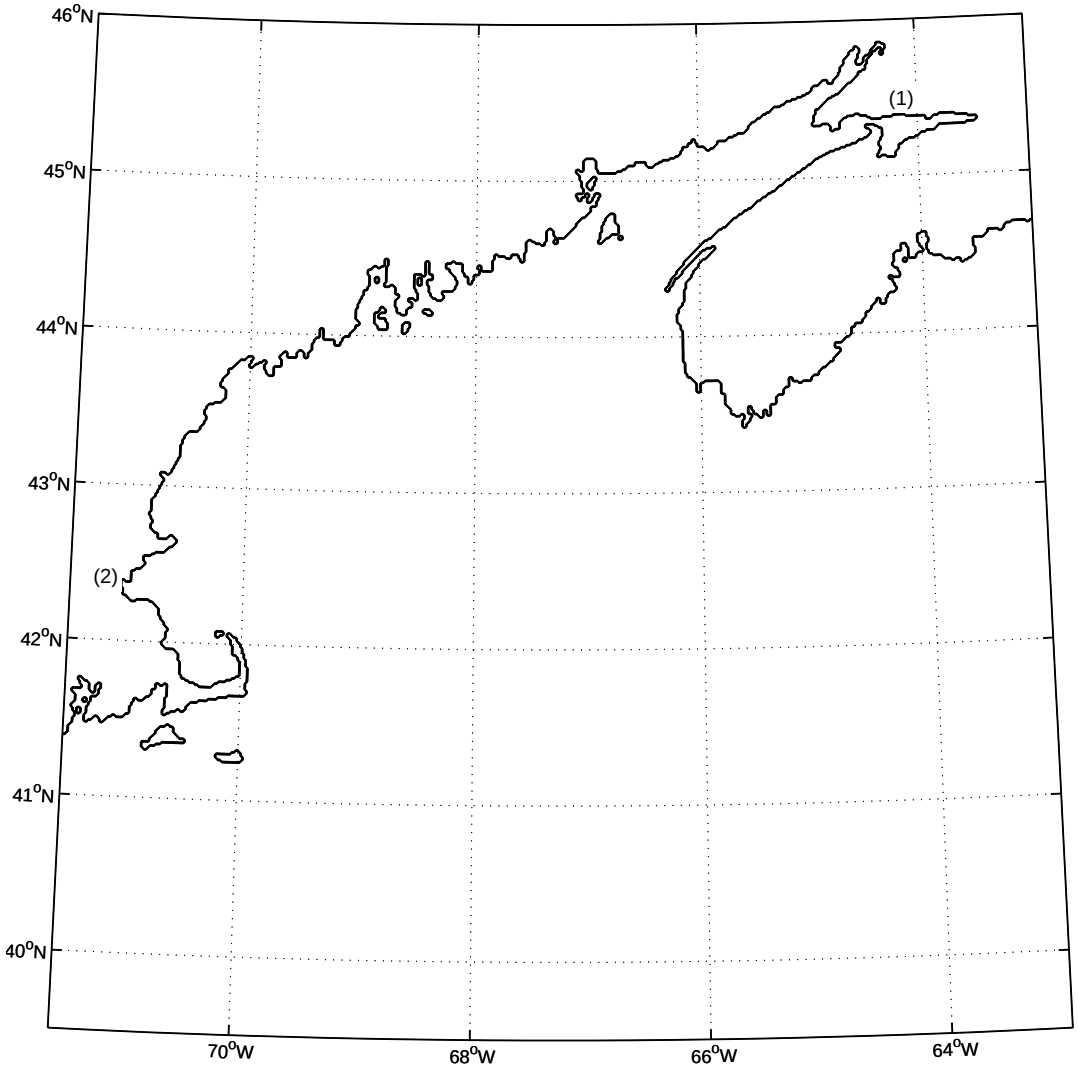

Figure 3.16. Map showing the location of Minas Basin (1) and Boston (2).

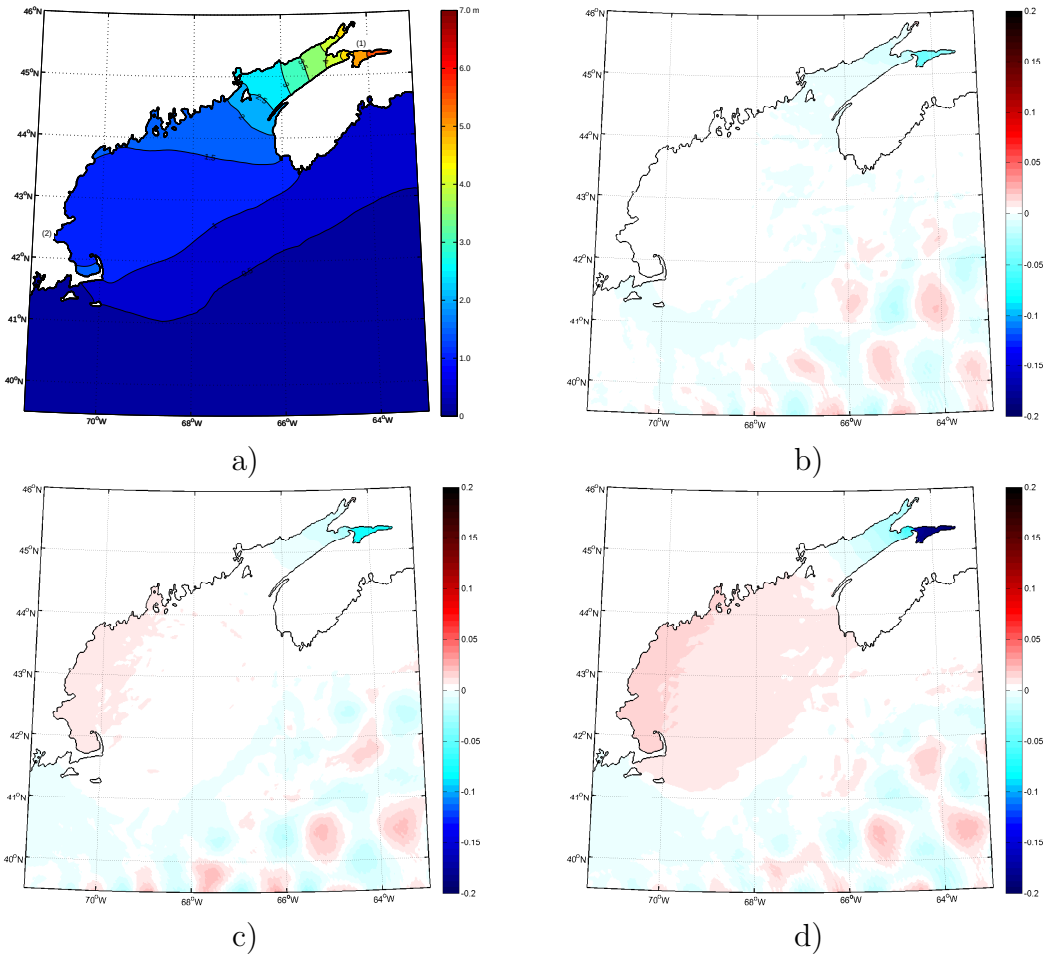

Figure 3.17. Impact of energy extraction scenarios on the amplitude of the M2 components. a) Present day amplitude (m); b) Changes in the M2 amplitudes due to 740 MW energy extraction scenario (m); c) Changes in the M2 amplitudes due to 1.23 GW energy extraction scenario (m). d) Changes in the M2 amplitudes due to 2.50 MW energy extraction scenario (m). Changes in amplitude are relative to the M2 amplitude at present day (a).

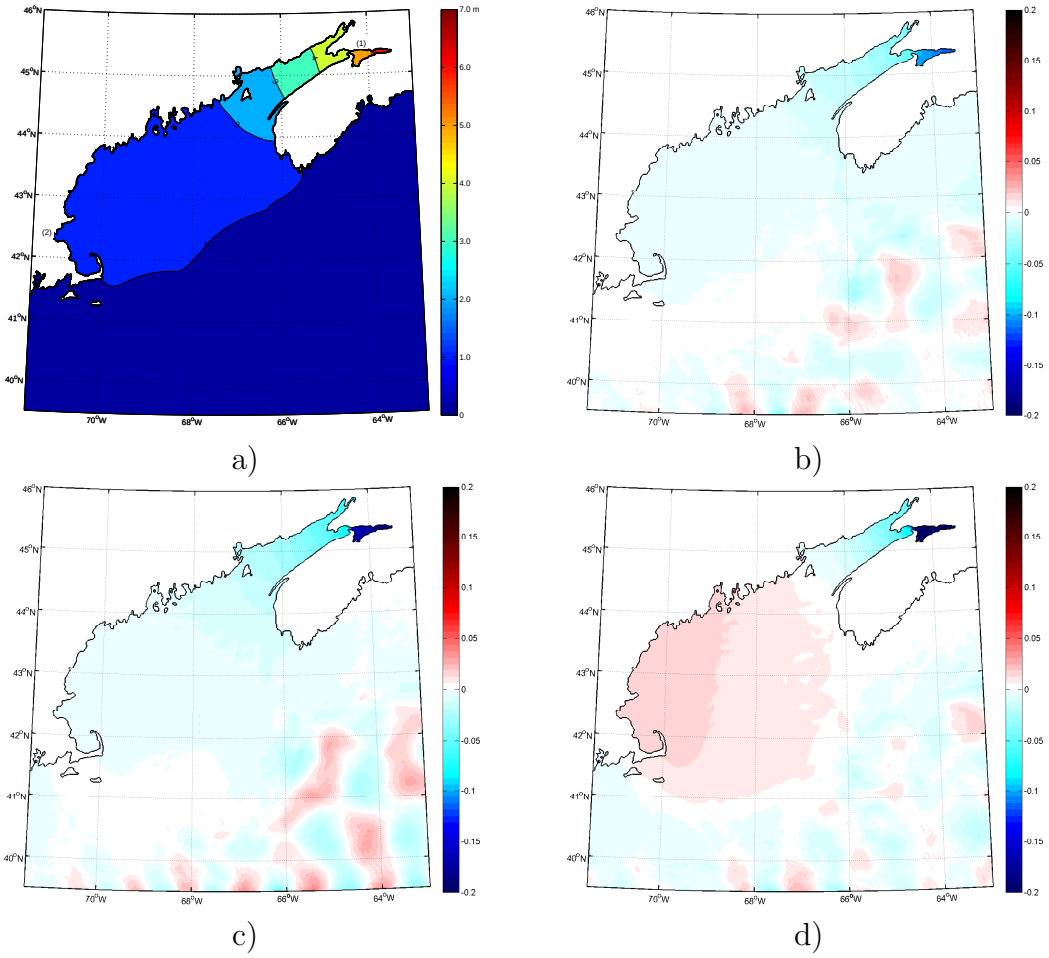

Figure 3.18. Impact of energy extraction combined with SLR scenario. a) The M2 amplitude for +1 m SLR scenario (m); b) Changes in the M2 amplitudes due to 740 MW energy extraction and SLR (m) scenario; c) Changes in the M2 amplitudes due to 1.23 GW energy extraction and SLR scenario (m). d) Changes in the M2 amplitudes due to 2.50 MW energy extraction and SLR scenario (m). Changes in amplitude are relative to the M2 amplitude for +1 m SLR scenario (a).

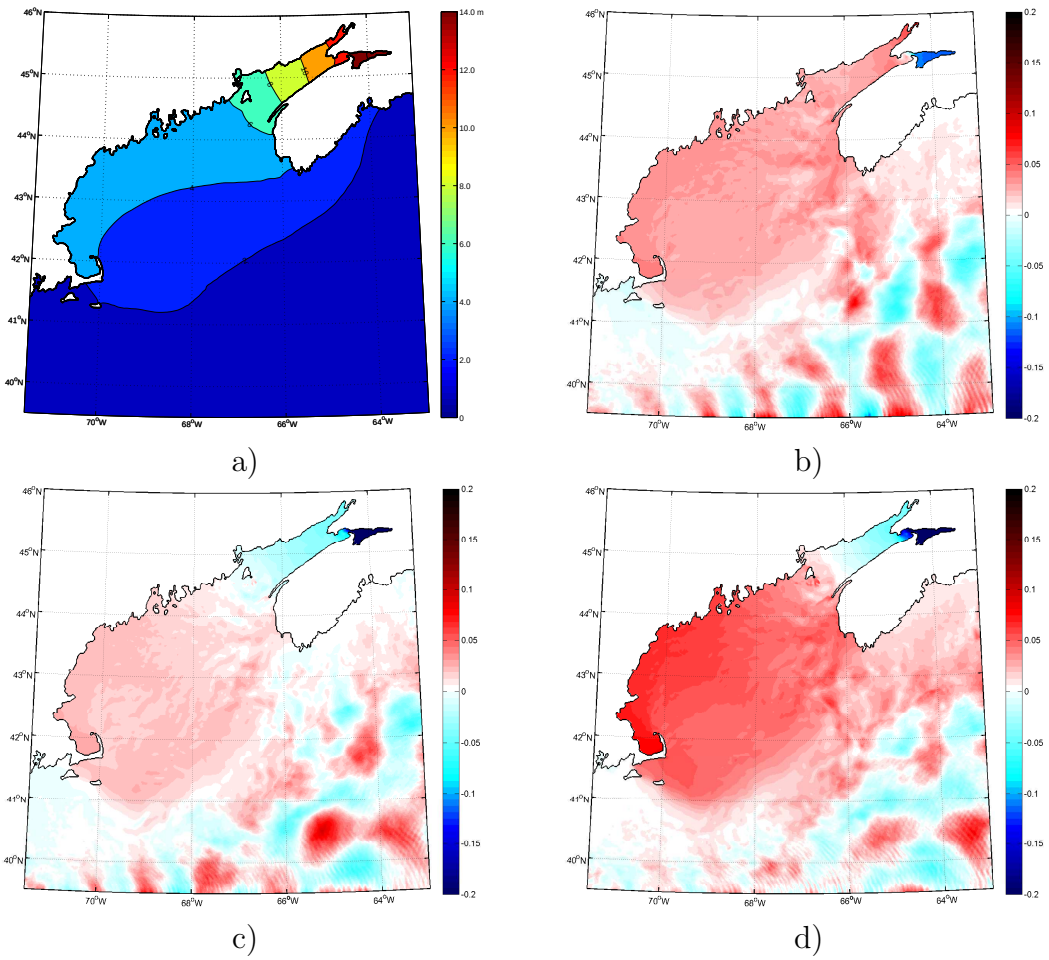

Figure 3.19. Impact of energy extraction scenarios on the tidal range. a) Present day tidal range (m); b) Changes in the tidal range due to 740 MW energy extraction scenario (m); c) Changes in the tidal range due to 1.23 GW energy extraction (m) scenario. d) Changes in the tidal range due to 2.50 MW energy extraction scenario (m). Changes in the tidal range are relative to the present day tidal range (a).

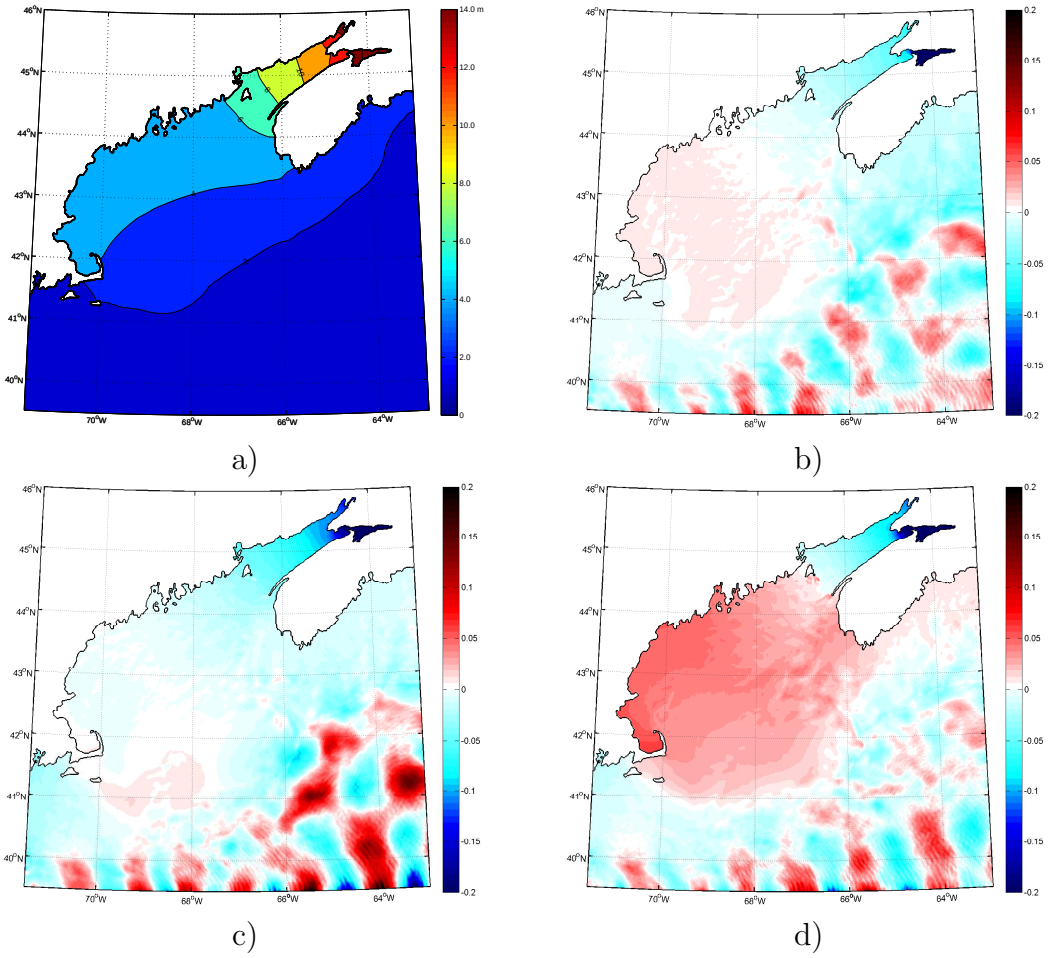

Figure 3.20. Impact of energy extraction scenarios on the tidal range. a) The tidal range for +1 m SLR scenario (m); b) Changes in the tidal range to 740 MW energy extraction and SLR scenario (m); c) Changes in the tidal range due to 1.23 GW energy extraction and SLR scenario (m). d) Changes in the tidal range due to 2.50 MW energy extraction and SLR scenario (m). Changes in amplitude are relative to the tidal range for + 1 m SLR scenario (a).

CHAPTER 4

Discussion

Throughout this effort, tidal-stream energy assessment, and the impact of tidal energy extraction and SLR in the Gulf of Maine have been explored. It is shown that SLR, as well as tidal energy extraction, are affecting the dynamics of tides in this region.

Application of ROMS in this study demonstrated convincing results to simulate ocean dynamics. Lewis et. al (2013) considered $\sim$1 km grid as sufficient resolution to assess the first TEC generation and suggested higher resolution for better simulation results. Based on model validation, the implementation of regular horizontal uniform 1 arc-minute grid ($\sim 1km^2$) in the Gulf of Maine shows good results for 3-D regional tidal simulation. For instance, 7% and 9% scatter index for validation of M2 component amplitude and phase, respectively. Further, higher resolution using regular horizontal grid and/or the implementation of sub grids may present better results for both tidal water elevation and tidal current velocity simulation in the domain, which has a very complex bathymetry and topography. However, the implementation of very high resolution and sub grid are complex and computationally more expensive.

Regarding the tidal-stream resource assessment, the inclusion of SLR scenario in this study: +1 m uniform water level and boundary effect, significantly affects the resource compared to the present day. In the Gulf of Maine, the effects of +1 m SLR to the bathymetry of the domain is relatively very small throughout the domain. Recent research in global ocean dynamics suggested that SLR not only affects the bathymetry, but also the dynamics of tides. According to Wilmes (2016) , about 10% increase in M2 amplitude was predicted due to + 1 m global uniform

SLR. Consequently, the implementation of the effects of SLR on tidal dynamics along the open ocean boundary become important as the tidal model is forced by tidal components. The results predicted up to 74% changes in tidal-stream resources throughout the domain except Minas Passage, which is predicted to have 37% increase in the resources. Based on the results, future energy extraction may benefit from SLR in terms of the available resource.

The simulation of tidal energy extraction in Minas Passage was conducted with the increasing bottom friction method in ROMS. The method allows TEC array representation using added bottom drag coefficient in the tidal model. The method is relatively simple compared to the actuator disc concept in ROMS, which is recently proposed by Roc (2010). By using the increasing bottom drag coefficient method, the bottom drag coefficient of the domain is spatially modified in the designed location to represent TEC array. The method was tested and the energy flux calculation showed good results, 4% error, between the estimate of energy extraction and the total energy dissipation by additional friction at the seabed. However, the increasing bottom drag coefficient distribute the energy dissipation uniformly inside the cell area so that the method neglects the hydrodynamics effects in the near-field produced by the blades, which is not the objective of this study. The actuator disc concept in ROMS provides more advanced approach for TEC representation with turbulence correction at TEC array location. The proposed method is more complex in terms of domain discretization that uses sub grids between ocean grid ($\sim$ 1 km) and turbine grid ($\sim$ 20 m) and is also computationally more expensive.

The inclusion of SLR change the results of energy extraction scenario in Minas Passage. Based on the results (Table 3.10 and Table 3.11), the changes in tidal amplitude throughout the domain is relatively small at the present day. The inclu-

sion of SLR significantly affects the results as maximum difference rise up to 8% in Boston. In detail, the impacts of SLR on present day without energy extraction scenario dominated the change in tidal amplitude (up to 7% change). Furthermore, the combination of energy extraction scenario and SLR showed non-linear relation between them. Therefore, future energy extraction activity in Minas Passage need to be explored regarding several topics, such as, total energy extraction scenario, spatial area of turbine array, SLR value related to TEC lifetime design, and TEC array configurations.

CHAPTER 5

Conclusion

Ocean renewable energy resources (e.g, tidal range and tidal stream) can help reduce carbon emissions (Pelc and Fujita, 2002). Tidal power generation is highly site-specific and generally is feasible where tidal range and/or current velocity are large enough due to ocean environment such as amplification by sea bottom profile, funneling in estuaries, reflections by large peninsulas, headlands and resonance effects (Frau, 1993). The dynamics of tides in the Gulf of Maine are unique due to the tidal resonance, which generates the largest tidal range in the world (about 16 m). Accordingly, a number of previous studies have assessed the impacts of the tidal energy development in the Gulf of Maine. Further, due to the sea level rise (SLR), those impacts may also change during the project lifetime, which is usually more than 25 years. In this research, the impact of tidal energy extraction considering sea level rise was simulated.

A tidal model of the Gulf of Maine was developed using Regional Ocean Model System (ROMS) at one arcminute scale. Results show that tidal amplitudes in the far field change due to energy extraction. Up to 4% decrease in tidal range was estimated in Minas Basin due to the 2.5 GW extraction scenario without SLR. On Massachusetts coastal area, the impacts of the same scenario can be considered negligible, 0.94%. The results generally agree with previous studies that predicted decreased tidal range inside the Bay of Fundy and increased tidal range on Massachusetts coastal area. For instance, Karsten in 2008 simulated 5% tidal amplitudes increase on Massachusetts coastal area due to 2.5 GW extraction scenario at Minas Passage and Hasegawa in 2011 simulated up to 60 cm tidal range decrease inside the Bay of Fundy due to 2.0 GW extraction scenario. Including the

1 m SLR (considering the change in the bathymetry and boundary forcing) resulted in up to 7% and 4% tidal range increase on Massachusetts shoreline and Minas Basin, respectively, for both tidal range and the M2 components. The application of actuator disc theory in ROMS will be considered in the future. In summary, the implementation of modified boundary forcing due to SLR, which was ignored in the previous works, can change the results of the impact assessment. Table 5.1 shows the summary of the impacts of tidal energy extraction and SLR.

Based on the results, the far-field impact is more threatening in coastal regions of US. However, the impact of energy extraction in Minas Passage is relatively small. Compared to the model validation, the impacts were inside the uncertainty level of the model. For example, maximum change in Boston coastal area was calculated up to 1.65 %, which is inside the level of uncertainty in models, about 10 %. Furthermore, the impact of SLR on the dynamics of tides is much more than energy extraction assuming 2.5 GW extraction in Minas Passage.

Table 5.1. Summary of the impact of energy extraction and SLR scenarios on the M2 and the tidal range. The tidal range at the present day are 15.08 m and 4.54 m for Minas Basin and Boston, respectively. For the M2 component, the amplitudes at the present day are 5.24 m and 1.49 m for Minas Basin and Boston, respectively.

	Tidal range(%)		M2 component amplitude(%)	
Scenario	Minas Basin	Boston	Minas Basin	Boston
740 MW	-0.73%	0.85%	-0.86%	0.13%
1230 MW	-1.88%	0.59%	-1.49%	0.47%
2500 MW	-3.59%	1.65%	-3.42%	0.94%
SLR scenario:				
+1 m SLR and boundary effect	4.20%	6.40%	2.92%	4.20%
Energy extraction and SLR scenario				
740 MW and SLR	1.35%	4.39%	3.52%	6.54%
1230 MW and SLR	0.02%	4.28%	2.32%	6.46%
2500 MW and SLR	-0.48%	5.43%	0.97%	7.83%

Changes are relative to the present day scenario

LIST OF REFERENCES

Bahaj, A. S. (2011). Generating electricity from the oceans. *Renewable and Sustainable Energy Reviews*, 15(7):3399–3416.

Brooks, D. A. (2006). The tidal-stream energy resource in passamaquoddy–cobscook bays: a fresh look at an old story. *Renewable Energy*, 31(14):2284–2295.

Brooks, D. A. (2011). The hydrokinetic power resource in a tidal estuary: The kennebec river of the central maine coast. *Renewable energy*, 36(5):1492–1501.

Chowdhury, S., Zhang, J., Messac, A., and Castillo, L. (2013). Optimizing the arrangement and the selection of turbines for wind farms subject to varying wind conditions. *Renewable Energy*, 52:273–282.

Cornett, A., Cousineau, J., and Nistor, I. (2013). Assessment of hydrodynamic impacts from tidal power lagoons in the bay of fundy. *International Journal of Marine Energy*, 1:33–54.

Cornett, A., Durand, N., and Serrer, M. (2010). 3-d modelling and assessment of tidal current resources in the bay of fundy, canada. In *Proc. 3rd Int. Conf. on Ocean Energy*.

Desplanque, C. and Mossman, D. J. (2001). Bay of fundy tides. *Geoscience Canada*, 28(1).

Divett, T., Vennell, R., and Stevens, C. (2013). Optimization of multiple turbine arrays in a channel with tidally reversing flow by numerical modelling with adaptive mesh. *Philosophical Transactions of the Royal Society of London A: Mathematical, Physical and Engineering Sciences*, 371(1985):20120251.

Esteban, M. and Leary, D. (2012). Current developments and future prospects of offshore wind and ocean energy. *Applied Energy*, 90(1):128–136.

Frau, J. P. (1993). Tidal energy: promising projects: La rance, a successful industrial-scale experiment. *Energy Conversion, IEEE Transactions on*, 8(3):552–558.

Garrett, C. (1972). Tidal resonance in the bay of fundy and gulf of maine. *Nature*, 238:441–443.

Garrett, C. and Cummins, P. (2005). The power potential of tidal currents in channels. In *Proceedings of the Royal Society of London A: Mathematical, Physical and Engineering Sciences*, volume 461, pages 2563–2572. The Royal Society.

Greenberg, D. A. (1987). Modeling tidal power. *Scientific American*, 257:128–131.

Hagerman, G. and Bedard, R. (2006). Massachusetts tidal in-stream energy conversion (tisec): survey and characterization of potential project sites. *Electrical Power Research Institute EPRI-TP-003 MA Rev*, 1.

Hasegawa, D., Sheng, J., Greenberg, D. A., and Thompson, K. R. (2011). Far-field effects of tidal energy extraction in the minas passage on tidal circulation in the bay of fundy and gulf of maine using a nested-grid coastal circulation model. *Ocean Dynamics*, 61(11):1845–1868.

Hedström, K. S. (2012). *Technical manual for a coupled sea-ice/ocean circulation model (version 4)*. Citeseer.

Iyer, A., Couch, S., Harrison, G., and Wallace, A. (2013). Variability and phasing of tidal current energy around the united kingdom. *Renewable Energy*, 51:343–357.

Karsten, R. H., McMillan, J., Lickley, M., and Haynes, R. (2008). Assessment of tidal current energy in the minas passage, bay of fundy. *Proceedings of the Institution of Mechanical Engineers, Part A: Journal of Power and Energy*, 222(5):493–507.

Khan, M., Bhuyan, G., Iqbal, M., and Quaicoe, J. (2009). Hydrokinetic energy conversion systems and assessment of horizontal and vertical axis turbines for river and tidal applications: A technology status review. *Applied Energy*, 86(10):1823–1835.

Legrand, C. (2009). *Assessment of Tidal Energy Resource: Marine Renewable Energy Guides*. European Marine Energy Centre.

MarineCurrentTurbine. Seagen.

Müller, M. (2011). Rapid change in semi-diurnal tides in the north atlantic since 1980. *Geophysical Research Letters*, 38(11).

Multon, B. (2013). *Marine Renewable Energy Handbook*. ISTE. Wiley.

Neill, S. P., Hashemi, M. R., and Lewis, M. J. (2014). The role of tidal asymmetry in characterizing the tidal energy resource of orkney. *Renewable Energy*, 68:337–350.

NOAA (2016). Products / sea level rise maps.

Parris, A., Bromirski, P., Burkett, V., Cayan, D. R., Culver, M., Hall, J., Horton, R., Knuuti, K., Moss, R., Obeysekera, J., et al. (2012). *Global sea level rise scenarios for the United States National Climate Assessment*. US Department of Commerce, National Oceanic and Atmospheric Administration, Oceanic and Atmospheric Research, Climate Program Office.

Pawlowicz, R., Beardsley, B., and Lentz, S. (2002). Classical tidal harmonic analysis including error estimates in matlab using t_tide. *Computers & Geosciences*, 28(8):929–937.

Pelc, R. and Fujita, R. M. (2002). Renewable energy from the ocean. *Marine Policy*, 26(6):471–479.

Pelling, H. E. and Mattias Green, J. (2013). Sea level rise and tidal power plants in the gulf of maine. *Journal of Geophysical Research: Oceans*, 118(6):2863–2873.

Peterson, E. W. and Hennessey Jr, J. P. (1978). On the use of power laws for estimates of wind power potential. *Journal of Applied Meteorology*, 17(3):390–394.

Pham, C.-T. and Martin, V. A. (2009). Tidal current turbine demonstration farm in paimpol-brehat (brittany): tidal characterisation and energy yield evaluation with telemac. In *Proceedings of the 8th European Wave and Tidal Energy Conference, Uppsala, Sweden*, volume 710.

Pugh, D. and Woodworth, P. (2014). *Sea-Level Science: Understanding Tides, Surges, Tsunamis and Mean Sea-Level Changes*. Früher erschienen u.d.T.: Pugh, David: Tides, tsunamis and mean sea-level changed. Cambridge University Press.

Roc, T., Conley, D. C., and Greaves, D. (2013). Methodology for tidal turbine representation in ocean circulation model. *Renewable Energy*, 51:448–464.

Rourke, F. O., Boyle, F., and Reynolds, A. (2010). Tidal energy update 2009. *Applied Energy*, 87(2):398–409.

Sutherland, G., Foreman, M., and Garrett, C. (2007). Tidal current energy assessment for johnstone strait, vancouver island. *Proceedings of the Institution of Mechanical Engineers, Part A: Journal of Power and Energy*, 221(2):147–157.

Wilmes, S.-B. (2016). *The impact of large-scale sea-level changes on tides in the past, present and future*. PhD thesis, School of Ocean Sciences Bangor University.

BIBLIOGRAPHY

Bahaj, A. S., "Generating electricity from the oceans," *Renewable and Sustainable Energy Reviews*, vol. 15, no. 7, pp. 3399–3416, 2011.

Brooks, D. A., "The tidal-stream energy resource in passamaquoddy–cobscook bays: a fresh look at an old story," *Renewable Energy*, vol. 31, no. 14, pp. 2284–2295, 2006.

Brooks, D. A., "The hydrokinetic power resource in a tidal estuary: The kennebec river of the central maine coast," *Renewable energy*, vol. 36, no. 5, pp. 1492–1501, 2011.

Chowdhury, S., Zhang, J., Messac, A., and Castillo, L., "Optimizing the arrangement and the selection of turbines for wind farms subject to varying wind conditions," *Renewable Energy*, vol. 52, pp. 273–282, 2013.

Cornett, A., Cousineau, J., and Nistor, I., "Assessment of hydrodynamic impacts from tidal power lagoons in the bay of fundy," *International Journal of Marine Energy*, vol. 1, pp. 33–54, 2013.

Cornett, A., Durand, N., and Serrer, M., "3-d modelling and assessment of tidal current resources in the bay of fundy, canada," in *Proc. 3rd Int. Conf. on Ocean Energy*, 2010.

Desplanque, C. and Mossman, D. J., "Bay of fundy tides," *Geoscience Canada*, vol. 28, no. 1, 2001.

Divett, T., Vennell, R., and Stevens, C., "Optimization of multiple turbine arrays in a channel with tidally reversing flow by numerical modelling with adaptive mesh," *Philosophical Transactions of the Royal Society of London A: Mathematical, Physical and Engineering Sciences*, vol. 371, no. 1985, p. 20120251, 2013.

Esteban, M. and Leary, D., "Current developments and future prospects of offshore wind and ocean energy," *Applied Energy*, vol. 90, no. 1, pp. 128–136, 2012.

Frau, J. P., "Tidal energy: promising projects: La rance, a successful industrial-scale experiment," *Energy Conversion, IEEE Transactions on*, vol. 8, no. 3, pp. 552–558, 1993.

Garrett, C. and Cummins, P., "The power potential of tidal currents in channels," in *Proceedings of the Royal Society of London A: Mathematical, Physical and Engineering Sciences*, vol. 461, no. 2060. The Royal Society, 2005, pp. 2563–2572.

Garrett, C., "Tidal resonance in the bay of fundy and gulf of maine," *Nature*, vol. 238, pp. 441–443, 1972.

Greenberg, D. A., "A numerical model investigation of tidal phenomena in the bay of fundy and gulf of maine," *Marine Geodesy*, vol. 2, no. 2, pp. 161–187, 1979.

Greenberg, D. A., "Modeling tidal power," *Scientific American*, vol. 257, pp. 128–131, 1987.

Hagerman, G. and Bedard, R., "Massachusetts tidal in-stream energy conversion (tisec): survey and characterization of potential project sites," *Electrical Power Research Institute EPRI-TP-003 MA Rev*, vol. 1, 2006.

Hasegawa, D., Sheng, J., Greenberg, D. A., and Thompson, K. R., "Far-field effects of tidal energy extraction in the minas passage on tidal circulation in the bay of fundy and gulf of maine using a nested-grid coastal circulation model," *Ocean Dynamics*, vol. 61, no. 11, pp. 1845–1868, 2011.

Hedström, K. S., *Technical manual for a coupled sea-ice/ocean circulation model (version 4)*. Citeseer, 2012.

Iyer, A., Couch, S., Harrison, G., and Wallace, A., "Variability and phasing of tidal current energy around the united kingdom," *Renewable Energy*, vol. 51, pp. 343–357, 2013.

Karsten, R. H., McMillan, J., Lickley, M., and Haynes, R., "Assessment of tidal current energy in the minas passage, bay of fundy," *Proceedings of the Institution of Mechanical Engineers, Part A: Journal of Power and Energy*, vol. 222, no. 5, pp. 493–507, 2008.

Khan, M., Bhuyan, G., Iqbal, M., and Quaicoe, J., "Hydrokinetic energy conversion systems and assessment of horizontal and vertical axis turbines for river and tidal applications: A technology status review," *Applied Energy*, vol. 86, no. 10, pp. 1823–1835, 2009.

Legrand, C., *Assessment of Tidal Energy Resource: Marine Renewable Energy Guides*. European Marine Energy Centre, 2009.

Lewis, M., Neill, S., Robins, P., and Hashemi, M., "Resource assessment for future generations of tidal-stream energy arrays," *Energy*, vol. 83, pp. 403–415, 2015.

MarineCurrentTurbine. "Seagen." [Online]. Available: http://www.seageneration.co.uk/

Müller, M., "Rapid change in semi-diurnal tides in the north atlantic since 1980," *Geophysical Research Letters*, vol. 38, no. 11, 2011.

Multon, B., *Marine Renewable Energy Handbook*, ser. ISTE. Wiley, 2013. [Online]. Available: https://books.google.com/books?id=yv6cYlKjk5cC

Neill, S. P., Hashemi, M. R., and Lewis, M. J., "The role of tidal asymmetry in characterizing the tidal energy resource of orkney," *Renewable Energy*, vol. 68, pp. 337–350, 2014.

Nicholls, R. J. and Cazenave, A., "Sea-level rise and its impact on coastal zones," *science*, vol. 328, no. 5985, pp. 1517–1520, 2010.

NOAA, "Products / sea level rise maps," 2016. [Online]. Available: http://www.star.nesdis.noaa.gov/sod/lsa/SeaLevelRise/

Parris, A., Bromirski, P., Burkett, V., Cayan, D. R., Culver, M., Hall, J., Horton, R., Knuuti, K., Moss, R., Obeysekera, J., *et al.*, *Global sea level rise scenarios for the United States National Climate Assessment*. US Department of Commerce, National Oceanic and Atmospheric Administration, Oceanic and Atmospheric Research, Climate Program Office, 2012.

Pawlowicz, R., Beardsley, B., and Lentz, S., "Classical tidal harmonic analysis including error estimates in matlab using t_tide," *Computers & Geosciences*, vol. 28, no. 8, pp. 929–937, 2002.

Pelc, R. and Fujita, R. M., "Renewable energy from the ocean," *Marine Policy*, vol. 26, no. 6, pp. 471–479, 2002.

Pelling, H. E. and Mattias Green, J., "Sea level rise and tidal power plants in the gulf of maine," *Journal of Geophysical Research: Oceans*, vol. 118, no. 6, pp. 2863–2873, 2013.

Peterson, E. W. and Hennessey Jr, J. P., "On the use of power laws for estimates of wind power potential," *Journal of Applied Meteorology*, vol. 17, no. 3, pp. 390–394, 1978.

Pham, C.-T. and Martin, V. A., "Tidal current turbine demonstration farm in paimpol-brehat (brittany): tidal characterisation and energy yield evaluation with telemac," in *Proceedings of the 8th European Wave and Tidal Energy Conference, Uppsala, Sweden*, vol. 710, 2009.

Pugh, D. and Woodworth, P., *Sea-Level Science: Understanding Tides, Surges, Tsunamis and Mean Sea-Level Changes*, ser. Früher erschienen u.d.T.: Pugh, David: Tides, tsunamis and mean sea-level changed. Cambridge University Press, 2014. [Online]. Available: https://books.google.com/books?id=QiBGAwAAQBAJ

Roc, T., Conley, D. C., and Greaves, D., "Methodology for tidal turbine representation in ocean circulation model," *Renewable Energy*, vol. 51, pp. 448–464, 2013.

Rourke, F. O., Boyle, F., and Reynolds, A., "Tidal energy update 2009," *Applied Energy*, vol. 87, no. 2, pp. 398–409, 2010.

Sutherland, G., Foreman, M., and Garrett, C., "Tidal current energy assessment for johnstone strait, vancouver island," *Proceedings of the Institution of Mechanical Engineers, Part A: Journal of Power and Energy*, vol. 221, no. 2, pp. 147–157, 2007.

Wilmes, S.-B., "The impact of large-scale sea-level changes on tides in the past, present and future," Ph.D. dissertation, School of Ocean Sciences Bangor University, mar 2016.

Wu, Y., Chaffey, J., Greenberg, D. A., Colbo, K., and Smith, P. C., "Tidally-induced sediment transport patterns in the upper bay of fundy: a numerical study," *Continental Shelf Research*, vol. 31, no. 19, pp. 2041–2053, 2011.